ARTICLE

Electron cryotomography analysis of Dam1C/DASH at the kinetochore–spindle interface in situ

Cai Tong Ng[1], Li Deng[1], Chen Chen[1], Hong Hwa Lim[2,3], Jian Shi[1], Uttam Surana[2,3,4], and Lu Gan[1]

In dividing cells, depolymerizing spindle microtubules move chromosomes by pulling at their kinetochores. While kinetochore subcomplexes have been studied extensively in vitro, little is known about their in vivo structure and interactions with microtubules or their response to spindle damage. Here we combine electron cryotomography of serial cryosections with genetic and pharmacological perturbation to study the yeast chromosome segregation machinery in vivo. Each kinetochore microtubule has one (rarely, two) Dam1C/DASH outer kinetochore assemblies. Dam1C/DASH contacts the microtubule walls and does so with its flexible "bridges"; there are no contacts with the protofilaments' curved tips. In metaphase, ~40% of the Dam1C/DASH assemblies are complete rings; the rest are partial rings. Ring completeness and binding position along the microtubule are sensitive to kinetochore attachment and tension, respectively. Our study and those of others support a model in which each kinetochore must undergo cycles of conformational change to couple microtubule depolymerization to chromosome movement.

Introduction

The spindle apparatus is a microtubule (MT)–based machine that partitions chromosomes equally between mother and daughter cells during mitosis. In yeast, the MTs in both the nucleus and cytoplasm are anchored by their closed "minus" ends to the nuclear envelope–embedded microtubule-organizing centers, termed spindle pole bodies. The MT "plus" end (the tips of the 13 protofilaments) can have either a flared or "ram's horn" configuration (Winey et al., 1995). Kinetochore MTs (kMTs) attach to chromosomes while the long pole-to-pole MTs give the spindle its characteristic shape. To prevent chromosome missegregation, cells use the spindle assembly checkpoint (SAC) to delay anaphase onset until two conditions are met: first, each sister chromosome must attach to kMTs emanating from one of the spindle pole bodies (Musacchio and Salmon, 2007); second, the spindle must generate tension via opposition between the kMT-induced poleward pulling forces and the cohesion between sister chromatids mediated by cohesin complexes (Michaelis et al., 1997). Chromosomes satisfying these two conditions have amphitelic attachments to the spindle and are considered bioriented. Damaged spindles and erroneous kMT attachments resulting in either unoccupied kinetochores or a loss of tension in the spindle apparatus leads to the activation of the SAC. The activated SAC imposes a transient cell cycle arrest in prometaphase, allowing cells to restore kinetochore-MT attachments before progressing to anaphase (Tanaka, 2010).

The kinetochore is a multi-functional protein complex that mediates the chromosome-kMT attachment and couples kMT depolymerization to poleward movement of the chromosome. Furthermore, the kinetochore is central to the SAC because it can assess the quality of chromosome-kMT attachment. Kinetochores are extremely complex. Traditional EM has defined a centromere-proximal "inner kinetochore" and a kMT-associated "outer kinetochore," each of which is assembled from multiple subcomplexes that have been studied individually (Musacchio and Desai, 2017). High-precision fluorescence imaging in vivo has revealed the composition and the average positions of many of these subassemblies (Joglekar and Kukreja, 2017). In yeast, the best understood one is the outer kinetochore Dam1C/DASH complex (Hofmann et al., 1998; Jones et al., 1999; Cheeseman et al., 2001; Janke et al., 2002; Li et al., 2002). 10 different polypeptides assemble as a Dam1C/DASH heterodecamer (Miranda et al., 2005). Dam1C/DASH heterodecamers can further oligomerize as rings around MTs (Miranda et al., 2005; Westermann et al., 2005). Owing to their circular shape and ability to form stable load-bearing attachments on MTs in vitro (Asbury et al., 2006; Westermann et al., 2006; Franck et al., 2007), Dam1C/DASH rings are thought to anchor the chromosome onto kMTs and couple kMT depolymerization to chromosomal poleward movement by interacting with the protofilaments' curved tips (Efremov et al., 2007).

[1]Department of Biological Sciences and Centre for BioImaging Sciences, National University of Singapore, Singapore; [2]Institute of Molecular and Cell Biology Agency for Science Technology and Research, Singapore; [3]Bioprocessing Technology Institute, Agency for Science Technology and Research, Singapore; [4]Department of Pharmacology, National University of Singapore, Singapore.

Correspondence to Lu Gan: lu@anaphase.org; C.T. Ng's present address is California Institute of Technology, Pasadena, CA.

Knowledge of kinetochore structure at the molecular level in vivo would shed light on fundamental questions that cannot be addressed by reconstitution. These questions include how the kinetochores couple to the kMTs, how the kinetochore subunits are oligomerized, how kinetochores are distributed in 3D within the spindle, and how both the kinetochore and spindle respond to perturbation. These structural details remain largely unknown in vivo because kinetochores are sensitive to conventional EM sample preparation methods (McEwen et al., 1998; McIntosh, 2005). Structural insights into large complexes like kinetochores and spindles in vivo require electron cryotomography (cryo-ET), which can reveal the 3D architecture of giant cellular machines and their subcomponents in a lifelike state (Gan et al., 2011).

We used cryo-ET of both serial and single frozen-hydrated sections (cryosections) of the budding yeast *Saccharomyces cerevisiae* to test decades-old structural models of chromosome-segregation in vivo (Hill, 1985; Efremov et al., 2007). We have examined the structure of yeast outer kinetochore Dam1C/DASH oligomers and their interactions with kMT walls (the outer surface that does not include the protofilaments' curved tips) in metaphase cells both with and without tension, in cells treated with a spindle poison, and in comparison to Dam1C/DASH-MT complexes in vitro. We found that Dam1C/DASH can oligomerize into partial and complete rings, both of which can associate with kMTs. Finally, our study reconciles different views concerning the mechanism of outer kinetochore function in a new model of MT-powered chromosome movement.

Results

Dam1C/DASH forms both complete and partial rings in vitro

To understand how individual Dam1C/DASH rings interact with MTs, we performed cryo-ET of plunge-frozen Dam1C/DASH assembled around MTs in vitro (Fig. 1, A and B; Miranda et al., 2005). We observed both complete and partial rings (Fig. 1, C and D). We define a ring as complete if the densities encircling the MT can be followed continuously through the 3D volume; therefore, distorted rings that have densities out of plane are also considered complete. Consistent with previous studies (Miranda et al., 2005; Westermann et al., 2005), our cryotomograms showed that all Dam1C/DASH rings are slightly tilted relative to the MT's axis. Furthermore, most of these complete and partial rings have flexible structures that connect the ring's rim to the MT walls (Fig. 1 E). These connections are called "bridges" (Westermann et al., 2005; Miranda et al., 2007; Wang et al., 2007) and are thought to be composed of parts of the Dam1p and Duo1p proteins (Zelter et al., 2015; Legal et al., 2016; Jenni and Harrison, 2018).

Rotational power spectra analyses (Murphy et al., 2006) of individual rings showed that most of the complete Dam1C/DASH rings had 17-fold symmetry in vitro (Fig. 2, A–G), like *Chaetomium thermophilum* Dam1C/DASH rings (Jenni and Harrison, 2018). This conclusion was further supported by asymmetric 3D class averages (no symmetry imposed), which also have 17-fold symmetry (Fig. 1 F and Fig. 2, I and J). Unlike in previous studies (Westermann et al., 2006; Wang et al., 2007; Ramey et al., 2011), we did not observe any 16-fold–symmetric rings in vitro; the reason for this difference is not clear. Nevertheless, our

Dam1C/DASH structure shares similar motifs with the previous ring structure (Ramey et al., 2011), such as the inward-pointing stump-like densities that correspond to a portion of the bridge (Fig. 1 G and Video 1) and densities extending from the ring's rim, parallel with the MT surface. These latter motifs correspond to the "protrusions" seen in *C. thermophilum* Dam1C/DASH rings (Jenni and Harrison, 2018). For brevity, herein we use the terms "bridge," "rim," and "protrusion" when referring to these prominent Dam1C/DASH structural motifs (Fig. 1 G).

Strategy to study yeast kinetochore structure in vivo

The in vivo structure of Dam1C/DASH is unknown. Previous tomography studies of high pressure–frozen, freeze-substituted cells revealed weak densities at kMT plus ends that might be partial or complete rings (McIntosh et al., 2013). To eliminate fixation, dehydration, and staining as sources of structural distortion, we prepared all our cells by high-pressure freezing, followed by cryomicrotomy to produce ~100–150-nm-thick cryosections. As a positive control, we assembled Dam1C/DASH rings around MTs in vitro and subjected these samples to the same high-pressure freezing and cryomicrotomy done for cells. The contrast of cryotomograms from such samples is extremely low due to the high concentration of the dextran cryoprotectant (Chen et al., 2016). Both partial and complete Dam1C/DASH rings were nevertheless visible in the resultant cryotomograms (Fig. 3 A). Note that some rings were distorted by cryosectioning, so that the entire ring could not fit in one tomographic slice. These rings could nevertheless be followed in 3D through adjacent slices (Fig. 3 B). Therefore, cryo-ET of cryosections can reveal both partial and complete Dam1C/DASH rings around kMTs if they exist in vivo.

One the greatest challenges in structural cell biology is the identification of the densities that belong to a protein complex in a cellular cryotomogram. This task cannot be done by immuno-EM because the sample was frozen and because immuno-EM uses a primary antibody–secondary antibody–gold complex, which is so long that any density within a 25-nm radius could be the protein of interest. Furthermore, immuno-EM requires cells to be fixed and stained, which perturb a protein complex's native structure. Some protein complexes can be localized by cryo-light microscopy, imaged by cryo-ET, and then identified by finding the structures that have the expected morphology (Chang et al., 2014; Bäuerlein et al., 2017). Alternatively, multi-megadalton protein complexes such as nuclear pores are confined to known subcellular positions and can be identified as the densities localized at the known position with the same structural signature (Albert et al., 2017). Kinetochore complexes can potentially be identified this way because they are located at the plus ends of kMTs.

We prepared mitotic yeast cells with either attached kinetochores under tension (metaphase), detached kinetochores without tension (nocodazole treated), or attached kinetochores without tension (Scc1-TEV268 cells; Fig. 4, A and B). A summary of the structural phenotypes observed in these cells is presented in Table 1. From these cells, we found Dam1C/DASH rings in 27 metaphase cells, of which 23 cells had at least three imageable serial cryosections; 3 nocodazole-treated cells; and 6 Scc1-TEV268 cells, of which 4 cells had at least three imageable serial cryosections. When Cdc20 is either depleted or rendered nonfunctional,
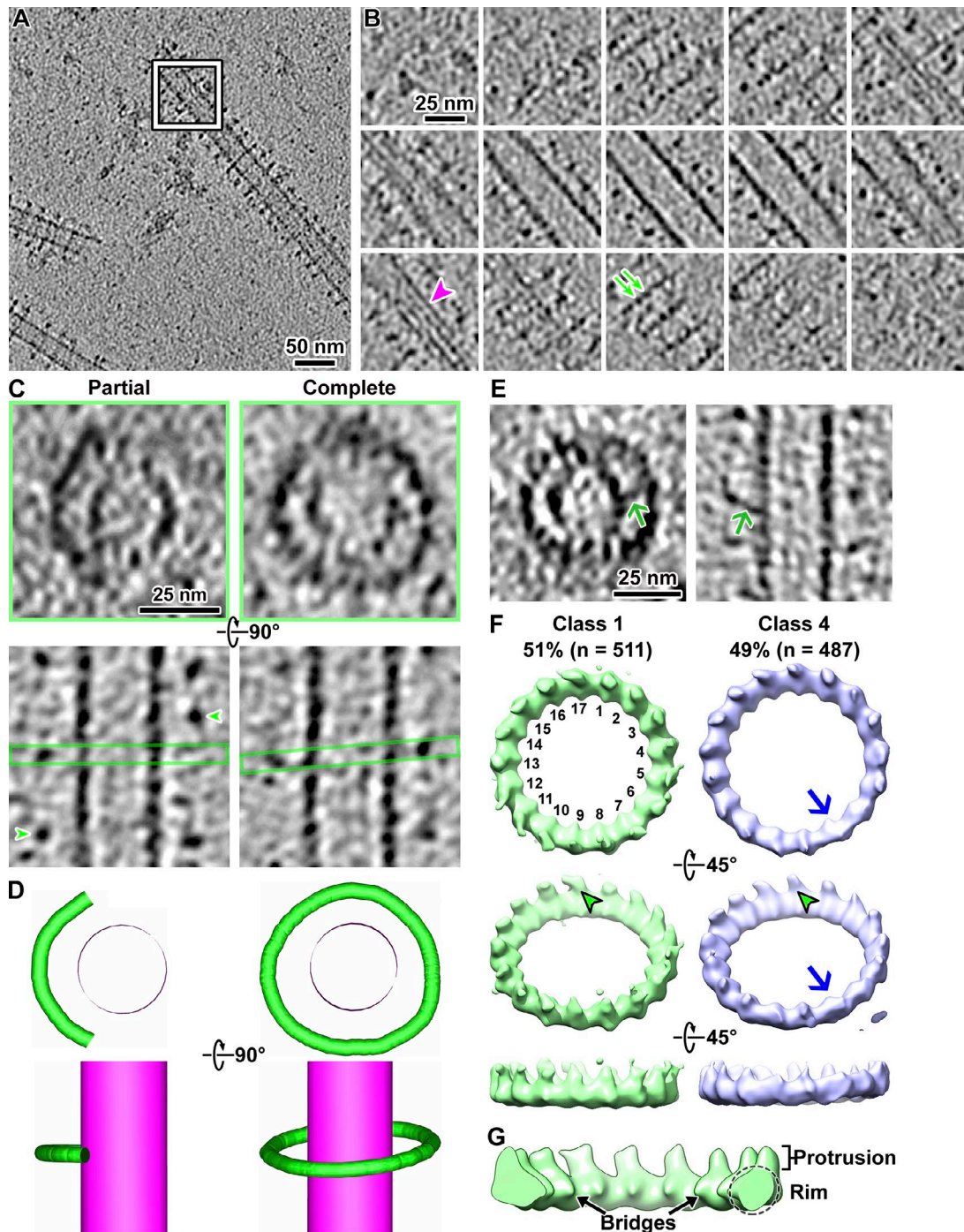
Figure 1. **Dam1C/DASH oligomerizes into partial and complete rings in vitro. (A)** Cryotomographic slice (60 nm) of MTs, encircled by Dam1C/DASH rings. The amorphous densities below and to the left of the white box are protein aggregates. **(B)** A series of cryotomographic slices (5 nm) through the position boxed in white in A, enlarged twofold. Magenta arrowhead: MT protofilament; green arrows: Dam1C/DASH decamers. **(C)** Cryotomographic slices (4.6 nm) showing front views of partial (left) and complete (right) Dam1C/DASH rings assembled around MTs. The bottom row shows the same rings but rotated 90° around the horizontal axis. Green arrowheads: densities of adjacent Dam1C/DASH oligomers; green boxes: approximate planes of the partial or complete ring taken in the top panels. **(D)** 3D models of Dam1C/DASH and MT complexes corresponding to top and bottom rows in C. **(E)** Two examples of Dam1C/DASH rings with bridges (green arrows), in the front (left) and side (right) views. **(F)** Asymmetric 3D class averages of Dam1C/DASH rings around MTs. Repeat subunits are numbered for class 1. Classes 2 and 3 (not shown) are very similar to class 4 and were included in the 49%. The top row is the front view. The middle and bottom rows are sequentially rotated 45° around the horizontal axis. Green arrowheads: protrusions; blue arrow: position in class average 4 that deviates from 17-fold symmetry. All density maps were masked to exclude the MT and contoured at 0.1 SD above the mean. **(G)** Enlarged, cutaway view of a 17-fold symmetrized Dam1C/DASH ring, with landmark motifs labeled. Note that the bridges appear shorter than in the individual subtomograms because their structures are extremely heterogeneous.
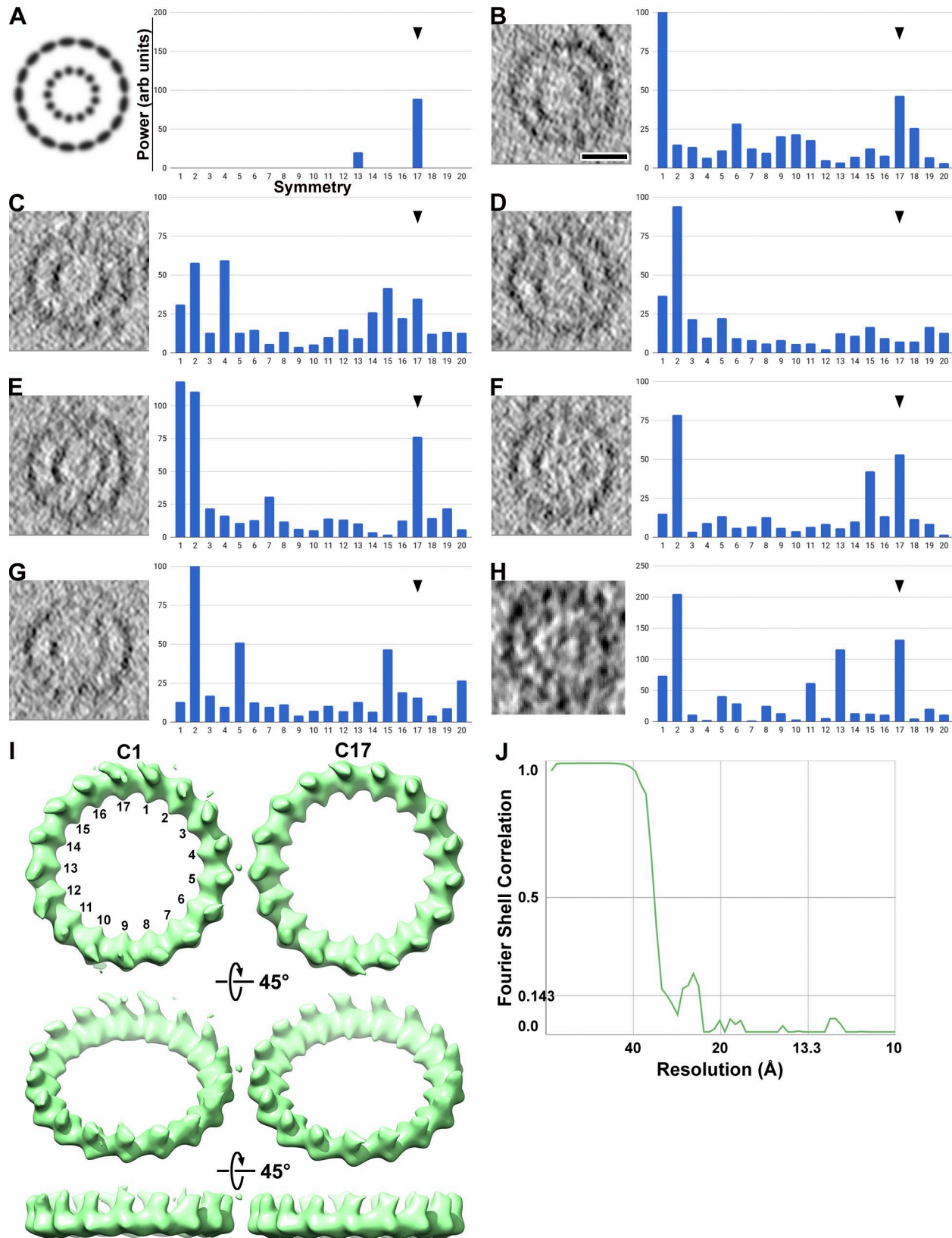
Figure 2. **Rotational symmetry analysis of Dam1C/DASH rings in vivo and in vitro. (A)** Left, manually constructed image with perfect 17-fold (outer) and 13-fold (inner) symmetries. The radii of the outer and inner arrays and their aspect ratios are to the approximate scales of a front view of Dam1C/DASH around MTs. Right, rotational power spectrum of the densities on the left. The y axis is the power (arbitrary units), and the x axis is the rotational symmetry. 17-fold symmetry is indicated by the black arrowhead. All subsequent plots have the same axes. **(B–G)** Left, cryotomographic slices of Dam1C/DASH ring around MTs in vitro, rotated to the front view. Right, power spectra of the cryotomographic slices. Bar, 25 nm for all cryotomographic slices. The non-Dam1C/DASH densities were masked before power spectrum analysis, but the mask is not shown. Some rings, such as those in D and G, are distorted and do not produce a strong

yeast cells arrest in metaphase with kinetochores attached to the spindle and under tension (O'Toole et al., 1997; Lau and Murray, 2012). To visualize kinetochores in metaphase, we arrested cells by depleting Cdc20 in a GAL-Cdc20 strain (Fig. 4 C). Because kinetochores take up a tiny fraction of the cell's volume, a single cryosection taken randomly through a cell is unlikely to contain a kinetochore. Indeed, our initial efforts to locate kinetochores in randomly sampled cryosections failed because we could not be confident whether a plus end belonged to a kMT or a polar MT. Serial cryosections in combination with serial cryo-ET can reveal a large enough volume that kMTs and their plus ends can be identified. Furthermore, serial cryo-ET can reveal intracellular heterogeneity of large complexes. We therefore devised a parallel bar grid–based serial-cryo-ET workflow that made possible the reconstruction of larger portions of spindles (Fig. 4, D and E; and Fig. 5A).

Dam1C/DASH forms both complete and partial rings around kMTs in vivo

We reconstructed portions of 23 metaphase spindles, each with at least three serial cryotomograms (most complete example in Fig. S1 and Video 2). We identified kMTs based on their short length, location, and orientation relative to the nuclear envelope (Fig. 5 B). Both complete and partial ring structures encircled the kMT plus ends (Fig. 5, C–F; additional examples in Fig. S2, A–C). We herein assign these complete and partial rings as Dam1C/DASH because their shape, diameter (47 ± 4 nm, mean and SD, $n = 14$ complete rings), localization at the kMT plus ends, bridge densities, and their absence from cytoplasmic MTs are all consistent with that expected of Dam1C/DASH from in vivo and in vitro studies (see below). The partial rings and complete rings have similar average radii of curvature (partial: 27 ± 3, $n = 19$; complete: 25 ± 2, $n = 17$; P = 0.27, two-tailed t test of unequal variance). Furthermore, the Cdc20 and Scc1-TEV268 partial rings did not differ in curvature (P = 0.13, $n = 8$ and 9; two-tailed t test of unequal variance). In terms of completeness, there was no dominant population in the partial rings, even when the metaphase and Scc1-TEV268 cells were considered separately (Fig. S2, D and E). Our most complete serial cryo-ET reconstruction contained nearly half a spindle with 13 Dam1C/DASH rings (Fig. 5 B and Videos 3 and 4). Budding yeast cells have 16 kinetochores per half spindle (one kinetochore per sister chromosome), so we probably missed three Dam1C/DASH rings due to the ambiguity of cryo-ET densities near the cryosection surfaces (14 surfaces in seven cryosections). The reconstruction is complete enough that we estimate that all kinetochores would fit into a rectangular volume <0.5 μm on a side (Fig. 5 C and Video 5). Cdc20-depleted cells have bigger spindles than wild-type cells (O'Toole et al., 1997). Notably, out of the 46 metaphase Dam1C/DASH complexes we

located, 28 (61%) were partial rings (Table 1). This observation is consistent with calibrated fluorescence light-microscopy data, which showed that there is not enough Dam1C/DASH to support 16 complete rings (average is only 12 Dam1C/DASH decamers per kMT; Dhatchinamoorthy et al., 2017). It is unlikely the partial rings are anything other than Dam1C/DASH because there are no other known outer kMT complexes that form curved structures that extend ~12 nm from kMT plus end's wall and are attached by bridge structures.

Dam1C/DASH bridges contact the kMT walls

Most kMTs had a single Dam1C/DASH ring (complete or partial, $n = 82$; Fig. 5, B and C). Only four kMTs had two partial Dam1C/DASH rings each (one example shown in Fig. 5 C). All rings were tilted relative to the kMT axis and the majority of them were positioned within 50 nm of the plus end. Both growing and shrinking MTs have curved protofilaments (McIntosh et al., 2018), so we could not distinguish between these two possible states. We did not observe any contacts between Dam1C/DASH and the back of the protofilaments' curved tips, which we define as any position where the protofilament's axis is perpendicular to the kMT axis. Instead, the only Dam1C/DASH–kMT interactions observed were between the kMT walls and Dam1C/DASH's bridges (Fig. 5, D–F; additional examples in Fig. 6). We also did not observe any contact between Dam1C/DASH and the back of the protofilaments' curved tips in vitro (Fig. S3). The Dam1C/DASH bridges are conformationally heterogeneous, even within the same ring, and could either be coplanar with the rim or curved out of plane (Fig. 5, D and E). If each Dam1C/DASH heterodecamer contributes a single bridge, then there would be up to 17 bridges per ring. In our combined in vivo and in vitro datasets, we observed at maximum 10 bridges per ring, meaning that some of the bridges were in as-yet-unknown conformations. This conformational flexibility explains how the bridge appears as a continuous density from the Dam1C/DASH rim to the MT surface in cryotomograms but as a stump-like density in multi-ring averages.

Two complete Dam1C/DASH rings in vivo had sufficient contrast to reveal that they had 17-fold symmetry (one analysis shown in Fig. 2 H). To better understand how Dam1C/DASH is organized in vivo, we symmetrized these two rings, yielding density maps with higher signal-to-noise-ratios (Fig. 5 G and Videos 6 and 7). These symmetrized rings have protrusions, which extend from the rim just like they do in rings in vitro (Fig. 1 F). In both instances, the protrusions point toward the kMT plus end and possibly interact with other kinetochore proteins. The surface opposite the protrusions is relatively featureless and also similar to the rings seen in vitro. As a control, we selected nine nuclear subtomograms and applied 17-fold symmetry and then masked and contoured them, all in the same way as for the

peak. The 15-fold symmetry peak comes from the MT densities (many MTs have 15 protofilaments in vitro), which can leak out of the mask due to the missing wedge effect. Note that because these cryotomographic slices were taken coplanar with the Dam1C/DASH ring, the symmetry signal from the MTs is weak or absent when the ring is tilted. **(H)** Left, cryotomographic slice (6 nm) showing the front view of a Dam1C/DASH ring around a MT in vivo. Right, rotational power spectrum. **(I)** Subtomogram averages of Dam1C/DASH rings around MTs, without (C1) or with 17-fold (C17) symmetry imposed. The unsymmetrized densities (C1) and subunit numbering are reproduced from Fig. 1 D. Only the most symmetric complexes, corresponding to those that resemble Class 1 in Fig. 1, were symmetrized. The top row is the front view. Each row below is sequentially rotated 45° around the horizontal axis. **(J)** On the basis of the Fourier-shell correlation = 0.143 criterion, the resolution of the 17-fold symmetrized reconstruction is 32 Å.
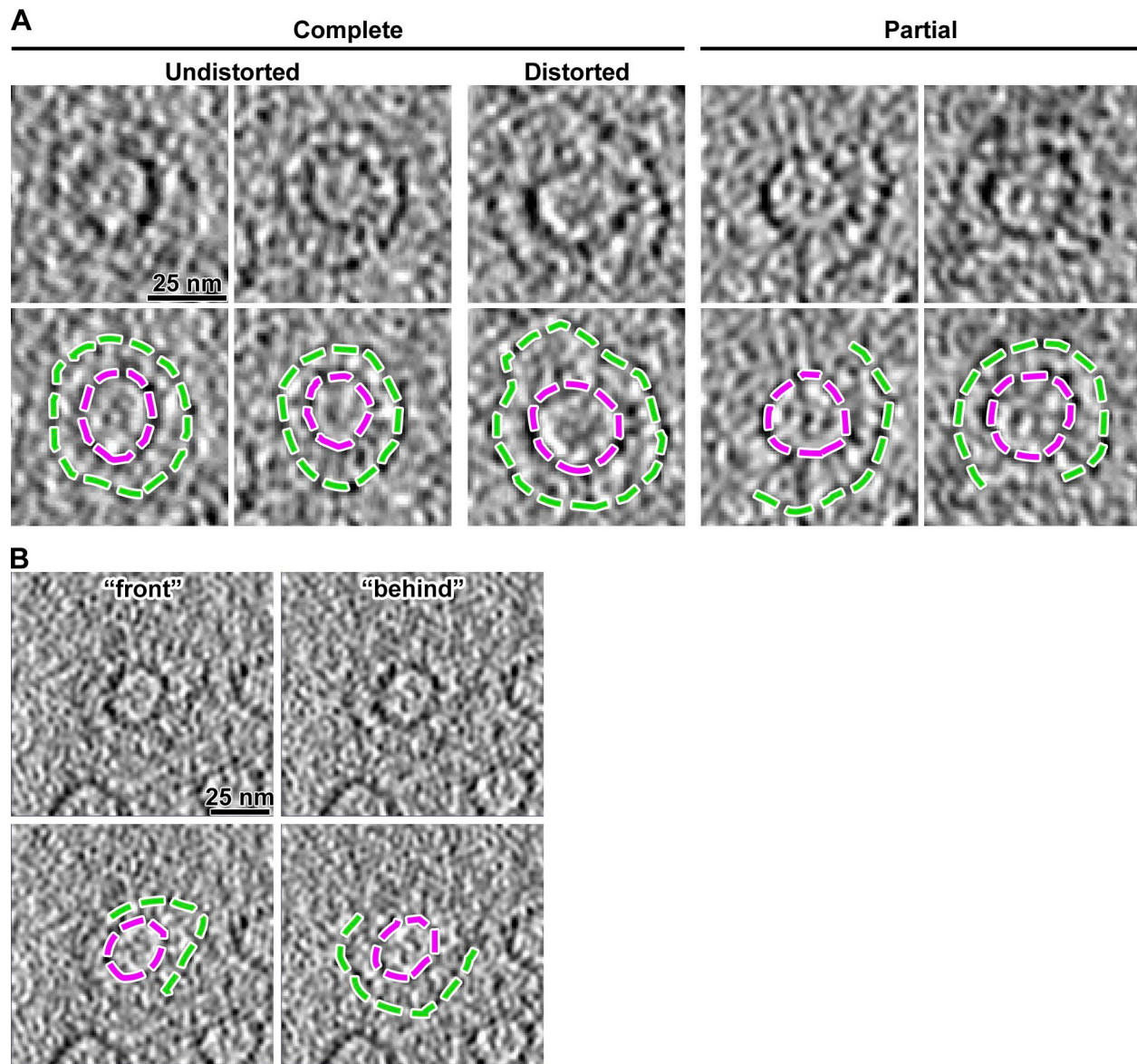
Figure 3. Dam1C/DASH rings can be visualized in cryosections. (A) Dam1C/DASH rings and MTs were assembled in vitro, high-pressure frozen, and then cryosectioned. Top row, cryotomographic slices (6 nm) of Dam1C/DASH rings around MTs. Bottom row, dashed lines corresponding to Dam1C/DASH (green) and MT (magenta) densities have been superposed on a copy of the top panel. **(B)** Some distorted Dam1C/DASH rings have portions that appear on different planes.

Dam1C/DASH rings. The resultant averages have nonsensical density arrangements (Fig. S3), further supporting our identification of Dam1C/DASH rings in vivo. From these symmetrized rings, we estimate that partial rings missing four or more Dam1C/DASH heterodecamers would have a gap large enough for a MT to pass through them (Fig. 5 G).

Unattached Dam1C/DASH forms partial rings, which remain clustered

Damaged spindles activate the SAC and can cause kinetochore detachment (Gillett et al., 2004). To test how spindle disruption affects kinetochore organization, we treated Dam1p-GFP–expressing cells with the spindle poison nocodazole and then imaged them by immunofluorescence microscopy (Fig. 7 A). Excluding a small subset of cells that lacked both Dam1C/DASH

and MT fluorescence signals, cells had either zero (18%, n = 41), one (63%, n = 143), or two punctate tubulin signals (13%, n = 30). Punctate MT fluorescence signals suggests that they are very short and form small clusters. Unlike MTs, all Dam1C/DASH fluorescence was confined to a single focus, suggesting that all the Dam1C/DASH rings formed a single cluster.

The intact spindle is a prominent landmark that facilitated our systematic search for kinetochores in metaphase-arrested cells; this strategy was not feasible in nocodazole-treated cells because spindles are disrupted. We therefore performed cryo-ET of 131 randomly chosen cryosections of these cells and were able to locate kMTs in five cryotomograms. Consistent with the immunofluorescence data, the nocodazole-treated cells contained small clusters of extremely short MTs (20–50-nm long; Fig. 7 B and Table 1), all of which had flared ends. In untreated cells,
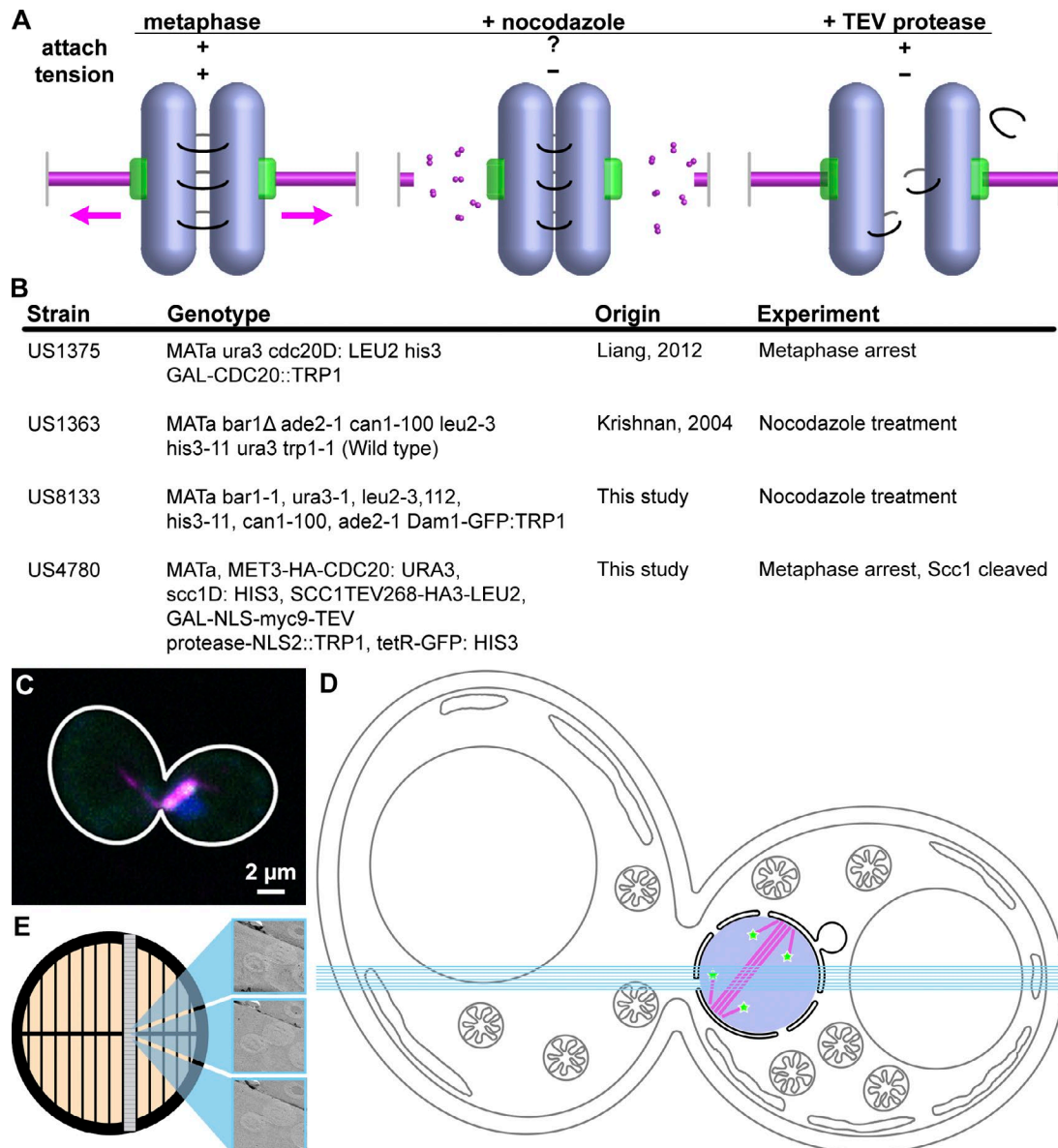
Figure 4. **Strategy to find kinetochores in vivo. (A)** Schematic of kinetochore states studied in this paper, not to scale. Sister chromosomes (pale blue pills) are held under tension (magenta arrows) in metaphase when kMT (magenta tubes) pulling forces are transmitted by cohesin (curved lines). Gray vertical bars: spindle-pole bodies. Tension at the kinetochores (green) can be eliminated either by the disruption of the kMTs with nocodazole or the conditional cleavage of mutant cohesin with TEV protease. This color scheme is used throughout the paper. **(B)** Strains used for this study, including those from previous studies (Krishnan et al., 2004; Liang et al., 2012). **(C)** Immunofluorescence image of a Cdc20-depleted cell, with Dam1p-GFP in green, tubulin in magenta, and DNA in blue. Owing to the merged channels, Dam1C/DASH appears white. **(D)** Cartoon of a mitotic yeast cell, with organelles drawn to approximate scale. The nucleus (pale blue circle), spindle (magenta lines), and kinetochores (green stars; not to scale) are colored. Cyan lines illustrate at scale a series of seven ~100-nm cryosections. **(E)** Serial cryo-ET strategy. Cryo-EM images of sequential cryosections of the same cell mounted on a parallel-bar grid are shown enlarged ~100-fold on the right.

cytoplasmic MTs have their plus ends near the cell membrane, making them extremely challenging to find in cryosections. Owing to their shortness in nocodazole-treated cells, the plus ends of four cytoplasmic MTs were seen in the vicinity of the nuclear envelope. Dam1C/DASH rings were found around some kMTs (nuclear) while cytoplasmic MTs did not have any Dam1C/DASH rings encircling them (Fig. 7, B–D; additional examples in Fig. S2). We saw one instance of the Dam1C/DASH rim in contact with the kMT wall (Fig. 7 D), but we did not see any Dam1C/DASH rings contacting the back of the protofilaments' curved

tips. Like in metaphase cells, Dam1C/DASH rings attached to kMT walls via flexible bridges. We also located small clusters of unattached Dam1C/DASH partial rings in the nucleoplasm, far from the spindle pole body (Fig. 7, E and F). Note that at the present resolution, we cannot distinguish whether a Dam1C/DASH complex is associated with a SAC protein–bound inner kinetochore. Our observations are consistent with the notions that kinetochores are clustered by an MT-independent mechanism (Goshima and Yanagida, 2000; Jin et al., 2000; Richmond et al., 2013) and that all 16 budding yeast kinetochores work together

Table 1. **Summary of observations**

Condition	Spindle	Attach	Tension	SAC	Dam1C/DASH rings			kMT
					Complete	Partial	n	nm
Metaphase	Intact	+	+	OFF	39%	61%	46	50–200+
Nocodazole treatment	MT stubs	+	–	ON	86%	14%	7	20–50
	Absent	–	–	ON	0%	100%	37	n/a
Metaphase, Scc1 cleaved; Scc1-TEV268	Distorted	+	–	ON	39%	61%	33	50–200+

n/a: kMT length unknown because they were not within the same cryosection as the kinetochore. Note that out of 86 attached Dam1C/DASH rings, kMT-tip-to-Dam1C/DASH distances could be measured for only 56 of them. Also, note that, due to the flexibility of the rings and the low contrast of cryotomograms, not every ring could be used to make both diameter and circumference/curvature measurements.

like a single, much larger mammalian kinetochore (Joglekar et al., 2008, 2009; Aravamudhan et al., 2014). In summary, some Dam1C/DASH subcomplexes detach from damaged spindles and are found as clusters of partial rings. Another subset of Dam1C/DASH rings encircle the extremely short kMTs and only contact the kMT's walls.

Kinetochore position on the kMT is sensitive to tension

Even if kinetochores are attached to kMTs, the spindle checkpoint can still be activated if tension across the spindle is lost. To determine how cells respond to loss of tension in the presence of attached kinetochores, we imaged metaphase cells in which cohesin can be conditionally cleaved. In these cells, Scc1 is replaced by Scc1-TEV268, which can be cleaved at an internal recognition site by inducible Tobacco Etch virus protease (Uhlmann et al., 2000; Mirchenko and Uhlmann, 2010; this paper). Note that we arrested these cells in a metaphase-like state by repressing the anaphase-promoting complex activator Cdc20 and then we cleaved Scc1-TEV268 by expressing TEV protease from a different promoter. These cells are not in true anaphase. Light micrographs showed that these cells have a large bud, extra long spindle, and a multi-lobed nucleus (Fig. 8 A). Our cryotomograms confirmed that these cells had distorted nuclei and also showed that MTs were absent from the center of the spindle (Fig. 8, B, F, and G). We located 33 Dam1C/DASH rings, which were much more difficult to find because longer kMTs made the plus ends appear less frequently in our cryotomograms and because many rings were located far from the kMT plus end in these cells (Fig. 8, C and D; additional examples in Fig. S2). Unlike in the other cells we imaged, Dam1C/DASH rings were rarely clustered; only one cluster was found in this dataset (Fig. 8 G). The ratio of complete to partial rings in these cells was similar to that in metaphase cells (Table 1).

In the absence of tension, some Dam1C/DASH rings were located very far (>100 nm) from the kMT plus ends. To test for a correlation between tension and the location of a Dam1C/DASH ring along a kMT, we measured the kMT tip to Dam1C/DASH distance for all three spindle conditions, with complete and partial rings kept as separate groups (Fig. 8 E). In metaphase cells with kinetochores under tension, there was no difference between the kMT tip to Dam1C/DASH distances in complete and partial rings (means and SDs: complete ring, 17 ± 18 nm and $n = 17$; partial ring, 24 ± 18 nm and $n = 26$; two-tailed t test P > 0.05). However, in the absence of spindle tension, a few partial rings were located much farther from the kMT plus ends than the complete rings. This broader kinetochore spatial distribution in Scc1-TEV268 cells with tensionless spindles is consistent with a previous study (Higuchi and Uhlmann, 2005). The complete rings in all three spindle states (metaphase, tensionless, and disrupted) were located close to the kMT plus end (disrupted spindle: 12 ± 6 nm, $n = 7$, two-tailed t test P > 0.05 for all pairwise comparisons). In summary, complete rings, but not partial rings, remain associated with the kMT plus end in the absence of tension.

Discussion

The discovery that the Dam1C/DASH outer kinetochore complex can form rings around MTs suggested a mechanism for how kinetochores can remain attached to a dynamic kMT tip (Hill, 1985; Miranda et al., 2005). Notably, a kMT-encircling complete ring is thought to be topologically trapped because its means of dissociation is the plus end, which is blocked by the protofilaments' curved tips. Structural studies have revealed a more complicated picture: Dam1C/DASH can also form spirals and partial rings (Wang et al., 2007; Gonen et al., 2012). Furthermore, calibrated fluorescence microscopy experiments revealed an average of 12 Dam1C/DASH heterodecamers per kinetochore (Dhatchinamoorthy et al., 2017), challenging the notion that the complete ring is the only functional form of Dam1C/DASH in vivo. Our study has now shown that partial and complete Dam1C/DASH rings coexist in the same cell, with partial rings being the majority species. In metaphase cells, 61% of the Dam1C/DASH rings were partial and 39% were complete. Many partial rings have gaps larger than 25 nm, meaning that those kinetochores are not stably attached to kMTs by topological means. Because partial rings are the majority form in vivo, they deserve closer scrutiny in future high-resolution in vitro studies. How would Dam1C/DASH keep chromosomes attached to spindles under tension? We believe that the strength of bridge–kMT interactions must be taken into consideration. Single-molecule studies suggested that Dam1C/DASH oligomers with only one to
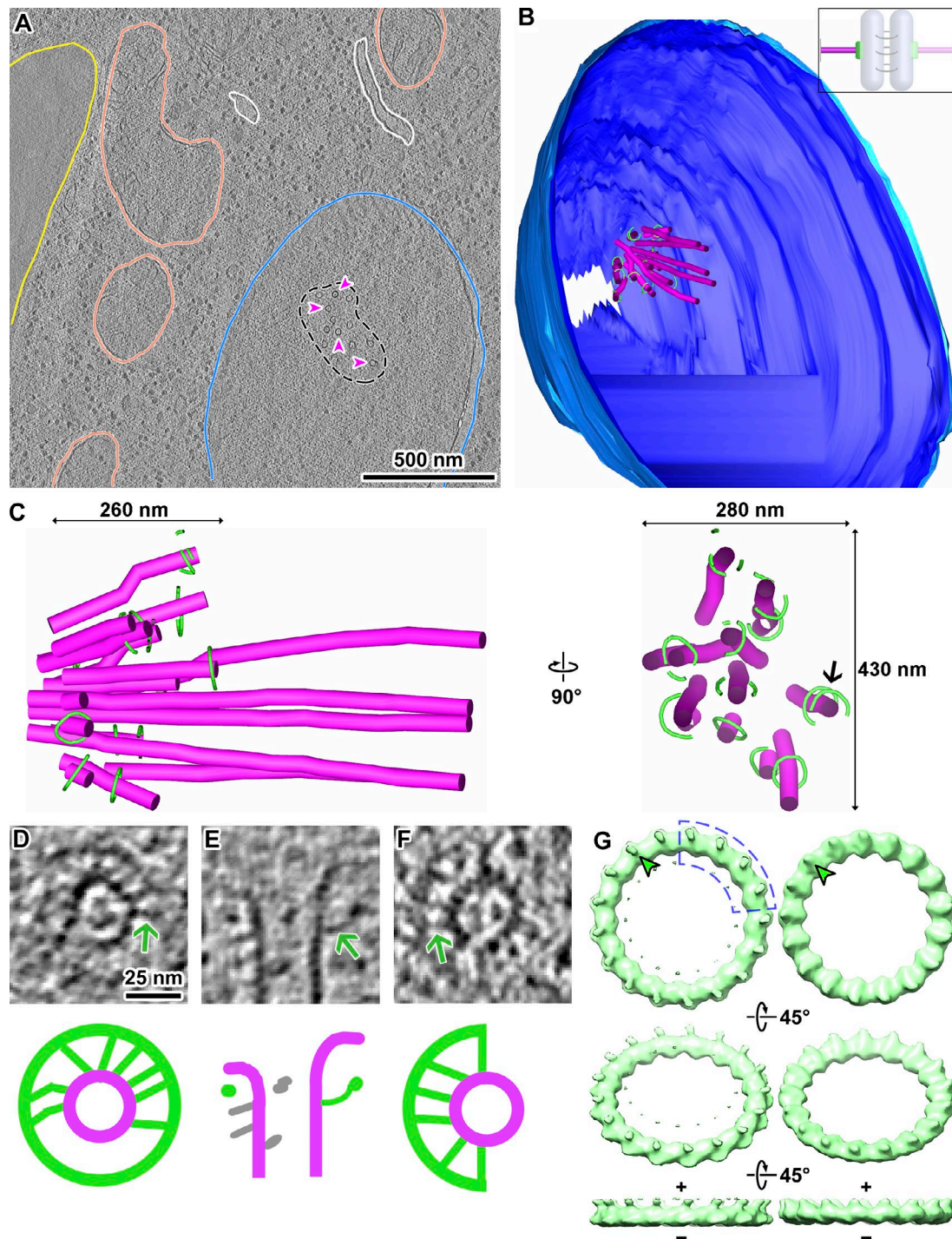
Figure 5. **Architecture of metaphase spindles and outer kinetochores. (A)** Cryotomographic slice (18 nm) from a Cdc20-depleted cell. Major features are annotated: cell membrane (yellow), mitochondria (salmon), endoplasmic reticulum (white), nucleus (blue). The black dashes outline the spindle. A few spindle MTs are indicated with magenta arrowheads. **(B)** 3D model of a half spindle, spanning seven sequential sections. Dark and light blue: inner and outer nuclear membranes. Magenta tubes: spindle MTs. Green rings: Dam1C/DASH. Inset: schematic showing the structures that are modeled (saturated shading) and those that are not (washed-out shading). **(C)** Left, enlargement of the spindle modeled in B and rotated to a view perpendicular to the spindle's axis. Right, transverse view of the same spindle; for clarity, polar MTs are omitted. Because the short axis crosses multiple cryosection interfaces, we are uncertain how long this spindle was in the unsectioned cell. This particular spindle also has an oval cross section due to microtomy compression along the x axis of the right panel. Black arrow: one example of a kMT with two partial rings. **(D–F)** Cryotomographic slices (6 nm) of Dam1C/DASH rings around kMTs. Green arrows point to bridges. The bottom panels show schematics of the Dam1C/DASH (green), kMT (magenta), and kMT-associated protein (gray) densities. D and F show front views of a complete and partial ring, respectively. E shows a side view of a complete ring. **(G)** Rotationally averaged density maps of two individual complete Dam1C/DASH rings in vivo, masked to exclude the kMT, contoured at one SD above the mean. Top row, front view. The middle and bottom rows are sequentially rotated 45° around the horizontal axis. Green arrowheads: protrusions. The plus and minus signs indicate the polarity of the encircled kMT. If four or more decamers (outlined by blue dashes) were absent, there would be a gap >25 nm.
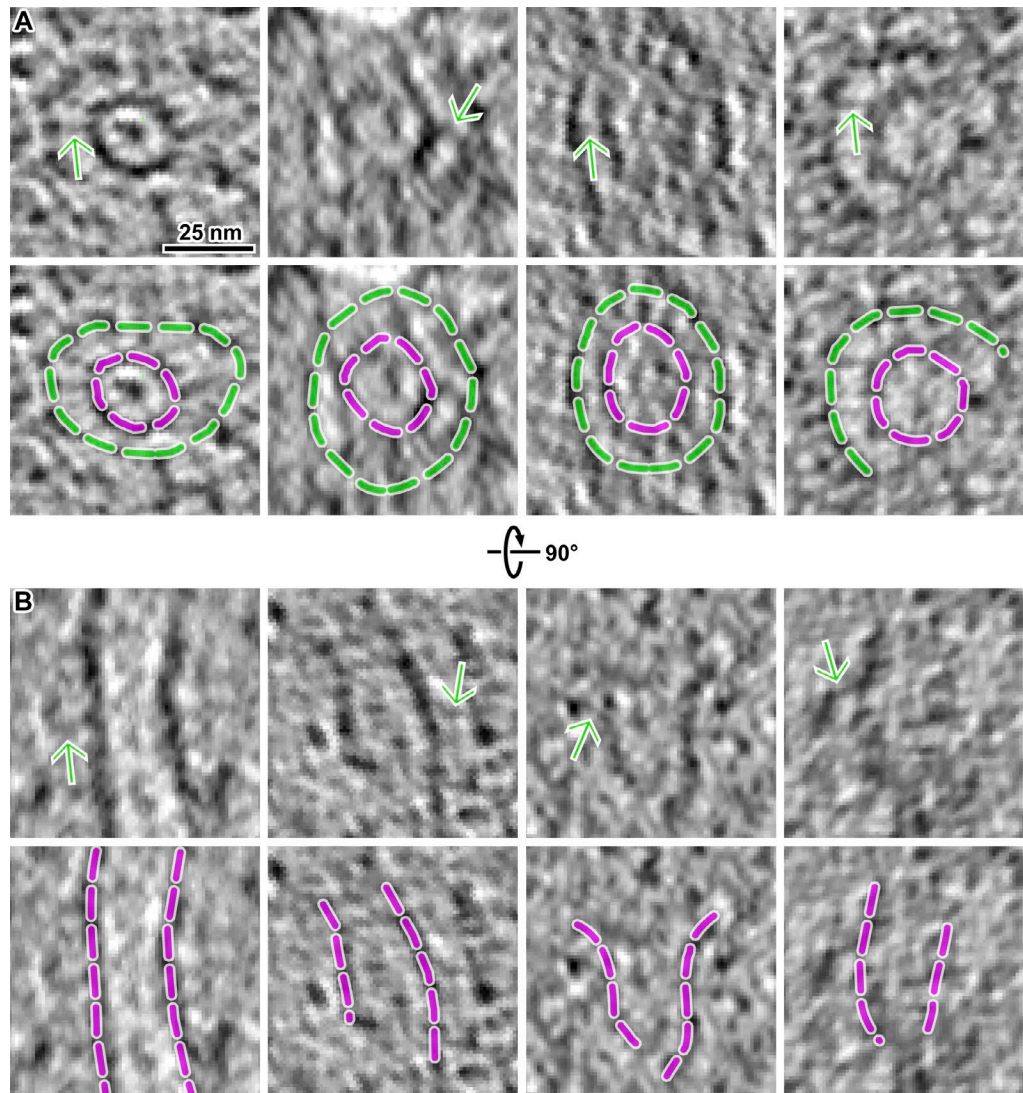
Figure 6.   **In vivo examples of Dam1C/DASH attachment to MT walls. (A)** Cryotomographic slices (5 nm) showing four examples of bridges (green arrows) on both complete and partial Dam1C/DASH rings (green dashes) attached to kMT walls (magenta dashes) in metaphase cells. Note: the kMT wall does not include the curved tips. For clarity, the top and bottom panels show the same densities but with different sets of annotations. **(B)** Same structures as in A, but rotated 90° around the horizontal axis.

four heterodecamers, which cannot be topologically trapped on a MT, can be pulled by depolymerizing MT plus ends (Gestaut et al., 2008). Furthermore, MT-bound Dam1C/DASH oligomers containing more than seven decamers have nearly undetectable diffusion (Volkov et al., 2013). Such stable interactions are also consistent with the observation that the MT-bound Dam1C/DASH pool does not exchange freely with the nucleoplasmic pool (Dhatchinamoorthy et al., 2017).

Comparison with in vitro studies

Dam1C/DASH has been studied extensively in vitro. Owing to the diversity of experimental conditions, these studies have produced varied results. Purified Dam1C/DASH can form either a complete ring, an incomplete ring, or a spiral when reconstituted around MTs, most frequently as densely packed sets of rings (Miranda et al., 2005; Grishchuk et al., 2008; Nogales and Ramey, 2009). The number of subunits that make up a complete

ring in such systems can range from 15 to 25 (Joglekar et al., 2006; Westermann et al., 2006; Miranda et al., 2007; Wang et al., 2007; Ramey et al., 2011; Jenni and Harrison, 2018). The bridge that connects Dam1C/DASH and MT walls (Miranda et al., 2007; Legal et al., 2016) has not been directly visualized. These bridges correspond to the Dam1p and Duo1p C-termini, and either appeared truncated or were absent from previous cryo-EM reconstructions because of their flexibility or removal from the expression construct (Wang et al., 2007; Jenni and Harrison, 2018). Our study suggests how consensus models (Alberts, 2015; Joglekar and Kukreja, 2017), which are largely based on in vitro studies, can be updated to depict the budding yeast mitotic machinery in vivo. Dam1C/DASH partial and complete rings should be shown making direct contact with the MT's walls, via bridges, which should number fewer than the Dam1C/DASH decamers (Fig. 9 A, top). In metaphase, these rings are all tilted and not making contact with the kMTs' curved protofilament tips (Fig. 9 A, bottom).
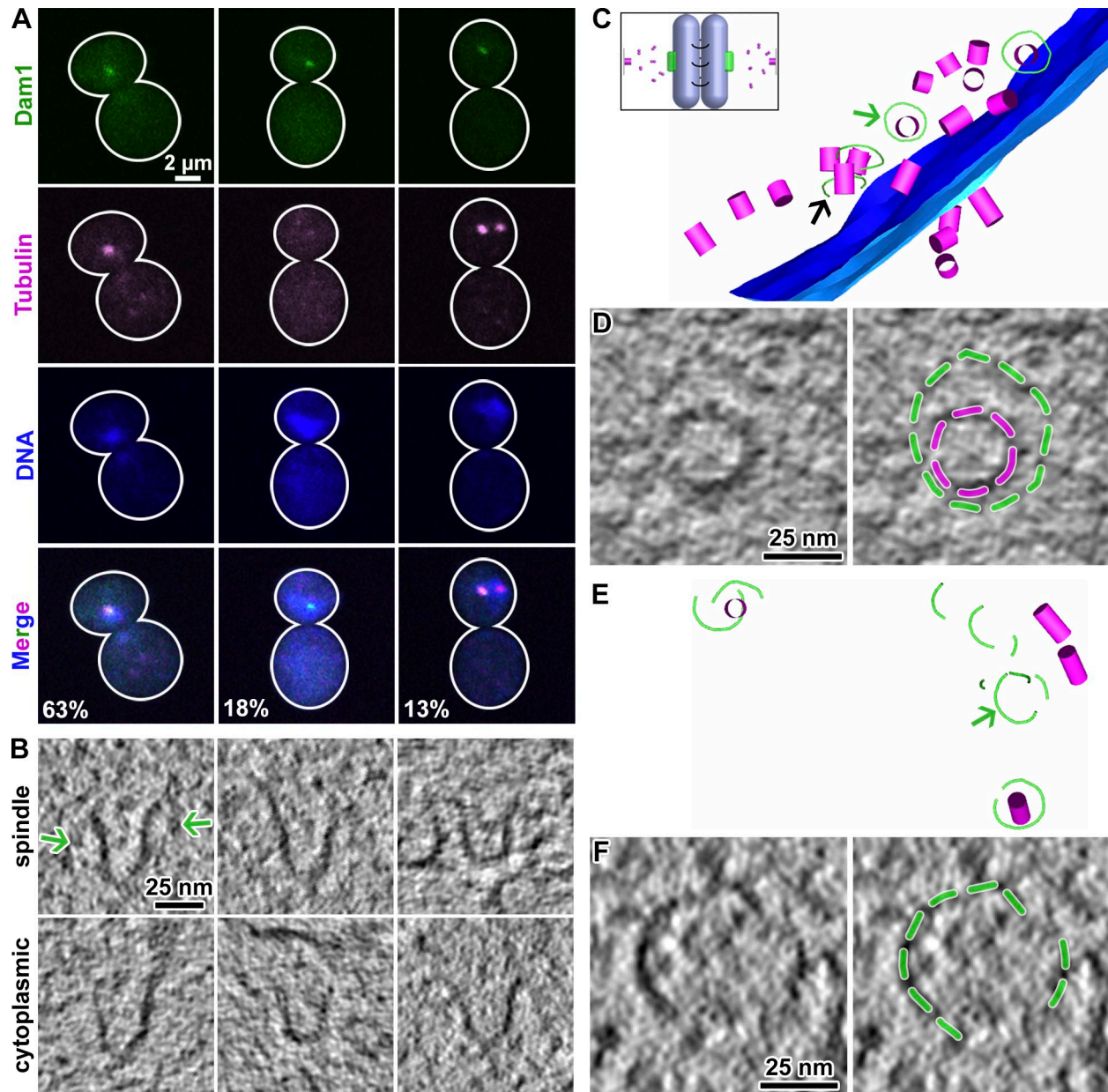
Figure 7. **Architecture of spindles in nocodazole-treated cells. (A)** Immunofluorescence images showing three major spindle morphologies in nocodazole-treated cells. A small minority of the cells had ambiguous morphologies and were not classified. The percentage belonging to each class is printed in the bottom row (*n* = 227). **(B)** Cryotomographic slices (10 nm) of spindle and cytoplasmic MTs. The plus end is oriented upward in each panel. Green arrows: Dam1C/DASH densities. **(C)** Model of a nocodazole-disrupted spindle with complete Dam1C/DASH rings associated with short MTs. Part of the bottommost Dam1C/DASH ring (black arrow) could not be modeled because it was located near the cryosection's surface. Green arrow: Dam1C/DASH ring that is enlarged in D. Inset: schematic showing the effect of nocodazole treatment. **(D)** Left, cryotomographic slice (8 nm) showing the front view of a complete Dam1C/DASH ring on a short kMT. Right, the same cryotomographic slice, but annotated with green dashes over the Dam1C/DASH densities and magenta dashes over the MT densities. **(E)** Model of unattached Dam1C/DASH oligomers and MT fragments in the nucleoplasm. Green arrow: partial Dam1C/DASH ring that is enlarged in F. **(F)** Left, cryotomographic slice (8 nm) showing unattached Dam1C/DASH partial rings. Right, the same cryotomographic slice but annotated with green dashes overlaying the Dam1C/DASH densities.

Kinetochores are commonly depicted as lone units, which gives the impression that each copy within a cell has the same structure. To better illustrate their conformational and compositional variability within cells, kinetochores should be depicted in groups, each instance with a Dam1C/DASH ring with a different level of completeness (Fig. 9 B). This change illustrates how the notion of the singular structure of a kinetochore component does not make sense in the context of the cell.

Dam1C/DASH is sensitive to both tension and attachment

Spindle integrity and tension at the kinetochore are thought to influence kinetochore structure, leading to SAC signaling. We have experimentally damaged the spindle of some cells and eliminated tension at the kinetochore of others. Our resultant analysis reveals that Dam1C/DASH is sensitive to both attachment and tension in these cells. Dam1C/DASH's oligomerization state in vivo depends on attachment but not tension: in the absence
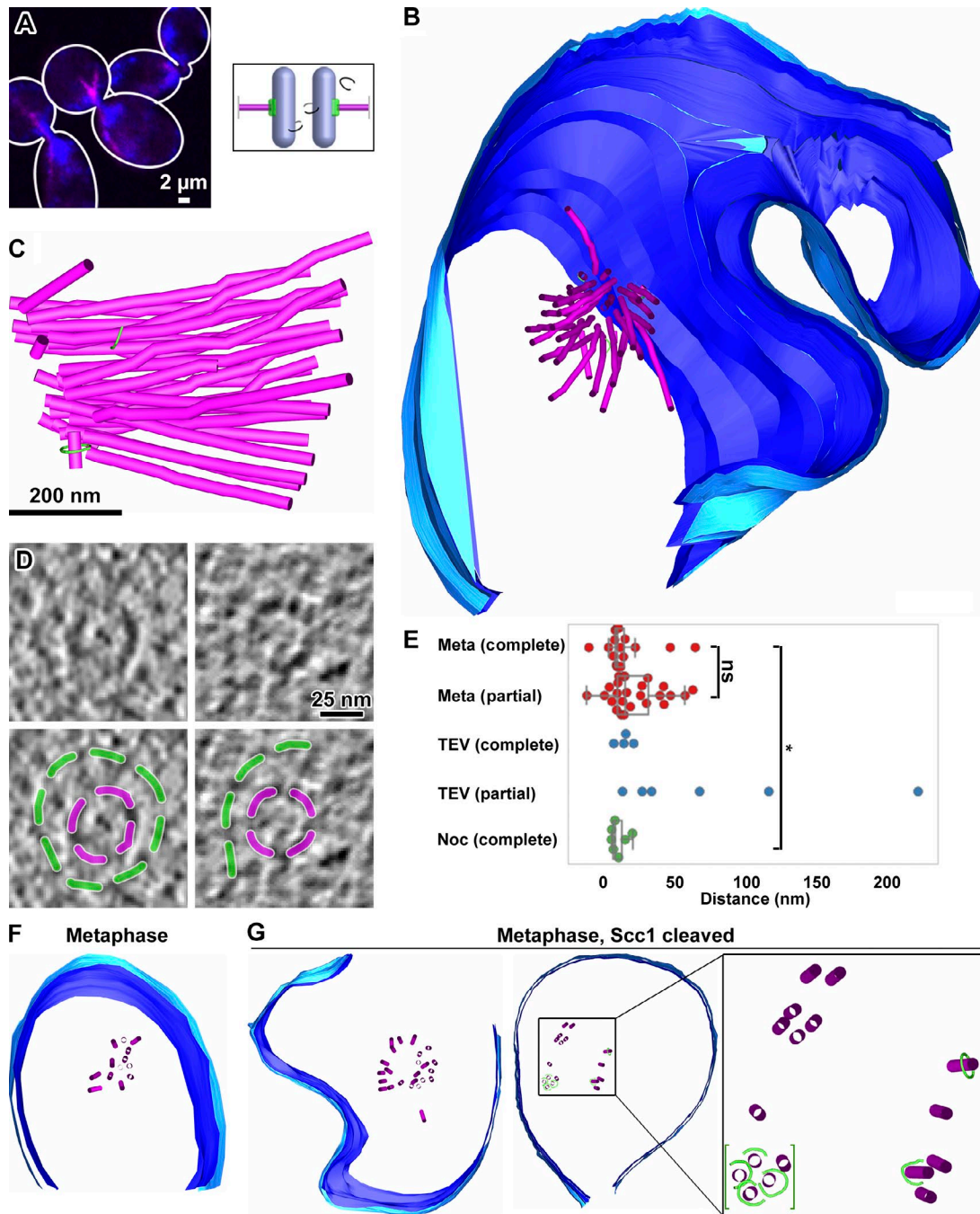
Figure 8. **Architecture of spindle machinery in mitotic cells without cohesion. (A)** Immunofluorescence image of metaphase-arrested cells (Cdc20 depleted) in which tension is absent because the cohesin subunit Scc1 is cleaved by TEV protease (Scc1-TEV268 cells). Blue: DNA. Magenta: MTs. Inset: schematic showing the loss of cohesion. **(B)** Serial cryo-ET model of one such cell. The nuclear envelope is colored blue and the spindle MTs colored magenta. The few Dam1C/DASH rings that were found are colored green. Note that the discontinuities in the nuclear envelope model are from the interfaces between adjacent cryosections, which could not be accurately modeled. **(C)** Enlargement of the spindle modeled in B, rotated to a view perpendicular to the spindle's axis. **(D)** Cryotomographic slices (6 nm) of front views of complete (left) and partial (right) Dam1C/DASH rings around kMTs. **(E)** Box-and-whisker plots and raw values (colored circles) of the distances between kMT plus ends and Dam1C/DASH ring centers of mass. Two Dam1C/DASH rings were located in front of kMT plus ends, which gave rise to negative distance values. Meta: cells arrested in metaphase (complete: $n = 12$; incomplete: $n = 8$). TEV: cells arrested in metaphase and with Scc1 cleaved (complete: $n = 4$; incomplete: $n = 5$). Noc: cells treated with nocodazole ($n = 3$). ns: not significant, Student's t test P > 0.05. Asterisk: F-test of equal variance P < 0.01. **(F)** A model of a portion of a metaphase spindle. MTs are magenta and the nuclear envelope membranes are blue. **(G)** Models of two metaphase spindles with Scc1 cleaved. These models came from single cryosections that were cut almost exactly transverse to the spindle axis. In metaphase cells without tension (Scc1 cleaved), the spindle MTs are arranged in isolated bundles surrounding a MT-free core. The spindle on the right (boxed) includes Dam1C/DASH rings (green) and is enlarged 3.5-fold on the right inset. Note that Dam1C/DASH rings within the cluster (green brackets) were spread out along the spindle axis (coming out of the image) and were not in contact.
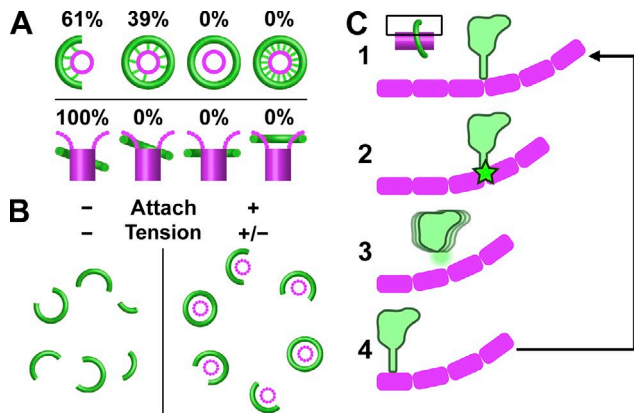
Figure 9. **A multi-scale model of the yeast mitotic machinery in vivo.** **(A)** The top half shows the types of Dam1C/DASH outer-kinetochore assemblies; left to right: partial rings, complete rings, complete ring without bridges, and complete ring with 17 bridges. The bottom half shows the possible position and tilt relationships between the Dam1C/DASH rings and the kMT plus end tips. The percent of each species observed in vivo is indicated. **(B)** Cartoon of clusters of Dam1C/DASH rings, viewed along the spindle axis. Dam1C/DASH (green) can only form complete rings when attached to kMTs (magenta). In the presence of attachment with or without tension, most of the rings are partial. **(C)** Inset: cartoon of a single Dam1C/DASH-kinetochore attachment site. The boxed area is enlarged, showing a schematic of Dam1C/DASH in cross section (green) and tubulin dimers (magenta rounded rectangles). The bridge is stably engaged with the MT wall (1) until the peeling protofilament becomes locally curved enough to destabilize the bridge's interaction (2). If enough Dam1C/DASH bridges are freed, the ring can locally diffuse along the kMT axis until it encounters a wall the MT (3). Here the bridge makes a stable contact again, attaching Dam1C/DASH to a position closer to the minus end (4).

of MTs, we only found partial rings (Fig. 9 B and Table 1). This observation suggests that Dam1C/DASH's oligomerization state in vivo depends on attachment but not tension. The kinetochores' positions (using Dam1C/DASH as a proxy) along the kMT's length is more complicated: they are located near the plus end in the presence of tension; without tension kinetochores with partial Dam1C/DASH rings can be found much farther from the plus end. How might these oligomerization and positioning differences be related to the SAC? An early fluorescence microscopy study showed that in nocodazole-treated cells, kinetochores far from the spindle pole body, but not those nearby, recruited checkpoint proteins (Gillett et al., 2004). In our cryotomograms of nocodazole-treated cells, detached kinetochores have detached partial Dam1C/DASH rings while the kinetochores still attached to the spindle remnant's short kMTs have mostly complete rings. These two findings suggest that the potentially interesting relationship between the SAC and kinetochore conformation and composition merits further cryo-ET investigation.

The yeast kinetochore is not a monolithic structure

Dam1C/DASH interacts with the KMN (Knl1, Mtw1, and Ndc80) outer kinetochore network and other kinetochore proteins, many of which have long coiled-coil domains (Westermann et al., 2005; Wang et al., 2008; Caldas and DeLuca, 2014). Such extended structures are "skinny" and would have been missed in our cryotomograms. However, globular domains such as the Ndc80 calponin-homology domain may account for some of the small densities protruding from kMT plus ends (Fig. 5 E). In the vicin-

ity of the kMT, there are also many nucleosome-sized densities, some of which may account for the centromeric nucleosome or the center of the hub-shaped MIND (Mtw1, Nnf1, Nsl1, and Dsn1) complex (Tachiwana et al., 2011; Gonen et al., 2012; Dimitrova et al., 2016). The centromeric nucleosome is expected to be coaxial with the kMT (McIntosh et al., 2013), but we did not observe any enrichment of nucleosome-sized or ribosome-sized densities along this axis. Instead, the majority of the kinetochores probably bind kMTs off-axis in vivo, which is also a phenotype of some purified kinetochores (Gonen et al., 2012). Our cryotomograms are consistent with a model in which the yeast kinetochore is a highly flexible structure and with its subcomponents spread over a large volume (Dimitrova et al., 2016; Jenni and Harrison, 2018).

A model for MT-driven chromosome movement

Yeast chromosomes move poleward along kMTs by two different mechanisms. Newly assembled yeast kinetochores first contact the side of a kMT and slide poleward by means of the kinesin Kar3 (Tanaka et al., 2005). Eventually, the kMT plus end contacts the kinetochore, leading to an "end-on" interaction and kMT-driven chromosome poleward movement (Tanaka et al., 2005, 2007; Kitamura et al., 2007). There are two popular models of kMT-driven poleward chromosome movement. In the ratchet model (Hill, 1985), kinetochores attach to the spindle by numerous weak interactions and undergo a random walk along kMTs, but have biased poleward movement by the receding plus end. In the forced walk model (Efremov et al., 2007), the depolymerizing protofilaments push a strongly bound kinetochore and force it to slide poleward. We did not observe any instance of Dam1C/DASH in contact with the protofilaments' curved tips in any of the three conditions, meaning that such contacts must be transient. We did frequently observe contacts between the Dam1C/DASH bridge and the MT's walls. To explain these observations, we propose a model that incorporates ideas from both the forced walk and ratchet models (Fig. 9 C). Steps 1 and 2: once the kMT protofilaments underneath Dam1C/DASH becomes curved enough, bridge detachment is triggered. Step 3: if a sufficient number of Dam1C/DASH heterodecamers lose contact, then the Dam1C/DASH ring can diffuse. Step 4, equivalent to step 1: once the Dam1C/DASH ring translates to a position where straight protofilaments are available, its bridges can reattach. As the kMT shortens, Dam1C/DASH heterodecamers must cycle between attached and detached states, biased poleward by transient steric interactions with the protofilaments' curved tips. In a partial ring, only a subset of the heterodecamers detach, meaning that the Dam1C/DASH rings might wobble as depicted in previous simulations (Efremov et al., 2007). Human kinetochores may also use this kMT-driven segregation mechanism if the functional homologue of Dam1C/DASH, called Ska1 (Hanisch et al., 2006; Welburn et al., 2009; Abad et al., 2014; Janczyk et al., 2017; van Hooff et al., 2017; Zhang et al., 2017), can switch rapidly between bound and unbound states. Furthermore, our model resembles an earlier one (Alushin et al., 2010). In that model, Ndc80 was proposed to form linear arrays aligned along the kMT axis in vivo. When phosphorylated, Ndc80 was proposed to sense the curvature of depolymerizing MTs and detach one at a time while the others remain clustered and attached to the un-curved portion of the MT surface. The structural predictions of MT-driven chromosome motion await further tests in vivo.

Materials and methods

Cell strains

All strains used in this study are detailed in Fig. 4 B.

Cell culture and metaphase arrest

Strain US1375 was grown in 50 ml YEPG (YEP: 10% yeast extract and 20% peptone, supplemented with 2% galactose and 2% raffinose) at 30°C, 250 RPM, to mid-log phase (OD_{600} = 0.5–1.0) before a change of growth medium to YEPD (YEP with 2% glucose). All growth-medium changes were done by draining YEPG with a vacuum filter, washing with twice the volume of YEPG and then resuspending the cells in YEPD. Next, the cells were kept in YEPD at 30°C for 3 h to arrest at metaphase. Right before self-pressurized freezing, the cells were checked by light microscopy for signs of large buds, which indicates successful metaphase arrest.

Metaphase arrest without cohesion

Strain US4780 was grown in YEPD without methionine overnight, then arrested in G1 phase by addition of α factor to 5 µg/ml. The cells were then washed free of α factor and then arrested at metaphase by incubation in YEP + raffinose + methionine medium for 4.5 h. Metaphase-arrested cells were then incubated in YEPG for 1.5 h to induce TEV protease expression. The induced cells were then placed on ice for 40 min during transportation to the cryo-EM facility for freezing.

Nocodazole arrest

Strains US1363 and US8133 were grown overnight in YEPD before arresting at G1 phase by incubation in YEPD containing 0.8 µg/ml α factor for 3 h. The arrested cells were then washed free of α factor and released into YEPD containing 15 µg/ml nocodazole. Cells were self-pressurized frozen after 4 h of incubation.

Immunofluorescence

Yeast cells were collected by pelleting 1 ml of liquid culture at 15,000 g for 1 min. The pellet was then fixed in KPF (100 mM K_2HPO_4 and 4% paraformaldehyde) at 22°C for 1.5 h. The cells were then washed three times with 1 ml 100 mM K_2HPO_4, then once with 1 ml SB (1.2 M sorbitol and 100 mM phosphate-citrate). Next, the cells were incubated at 30°C in 200 µl SB containing glusulase and zymolase for cell wall digestion. The resulting spheroplasts were washed with SB and then incubated with primary antibody (diluted 1:1,000) for 2 h at 22°C. After washing out the unbound primary antibody with BSA-PBS (1% BSA, 40 mM K_2HPO_4, 10 mM KH_2PO_4, and 150 mM NaCl), the spheroplasts were incubated with secondary antibody (diluted 1:2,000) for 2 h at 22°C. After washing out excess secondary antibody with BSA-PBS, the spheroplasts were suspended in 5 µl of mounting media (Vectashield H-1200; Vector Laboratories) and imaged using a Perkin Elmer UltraView Vox Spinning Disc confocal microscope equipped with an EM charge-coupled device camera C9100-50. Cells were imaged using Olympus UPLSAPO 60×/1.2 Water objective lens and images were acquired using Volocity. Light microscopy images were subsequently visualized using ImageJ (National Institutes of Health).

Dam1C/DASH expression, purification and assembly

Dam1C/DASH heterodecamers were expressed and purified using slightly modified published protocols (Miranda et al., 2005; Westermann et al., 2005). All protein buffers contained protease inhibitor (cOmplete; Sigma). The plasmid pC43HSK3H (Miranda et al., 2005) was transformed into BL21 Rosetta 2 (DE3) pLysS cells. This plasmid expresses all 10 Dam1C/DASH polypeptides (Dam1p, Dad1p, Dad2p, Dad3p, Dad4p, Duo1p, Ask1p, Spc19p, Spc34p, and Hsk3p). Cells were grown to OD_{600} = 0.4, then induced by addition of isopropyl β-D-1-thiogalactopyranoside to 1 mM. After 4 h of induction at 37°C, the cells were pelleted by centrifugation at 5,000 g for 15 min. The cells were resuspended in 30 ml sonication buffer (20 mM sodium phosphate, pH 6.8, 500 mM NaCl, 1 mM EDTA, 20 mM Imidazole, and 0.5% vol/vol Triton X-100) and lysed by sonication at 4°C for 5 min (power: 500 W; frequency: 20 kHz; amplitude: 35%; pulse: 0.5 s; elapsed: 0.5 s). The lysates were then centrifuged at 15,000 g for 30 min to remove the debris. Ni-NTA agarose beads (5 ml) were exchanged into sonication buffer by twice pelleting at 100 g for 2 min, then resuspending in sonication buffer. The Ni-NTA beads were then mixed with the lysates and incubated at 4°C for 2 h. Next, the Ni-NTA beads were pelleted by centrifugation at 2,000 g for 2 min and washed with sonication buffer twice. Elution buffer (20 ml) was added into the Ni-NTA beads and rotated overnight at 4°C at 200 RPM. The eluate was centrifuged at 100 g for 2 min. The supernatant was dialyzed to SP low-salt buffer (20 mM sodium phosphate, pH 6.8, 150 mM NaCl, and 1 mM EDTA) and concentrated to 1 ml. The concentrated eluate was loaded into a 1 ml HiTrap SP sepharose cation-exchange column. The fraction that eluted in 600 mM NaCl was further purified by gel filtration in a Superose 6 column in Superose buffer, which also functioned as the Dam1C/DASH storage buffer (20 mM sodium phosphate, pH 6.8, 500 mM NaCl, and 1 mM EDTA). The largest peak was concentrated to 1 ml using a Vivaspin concentrator (2 ml) and then aliquoted to 10 µl per tube. The aliquots were snap frozen with liquid nitrogen and stored at –80°C (Westermann et al., 2005).

Preparation of control Dam1C/DASH around MTs

Porcine tubulin (5 mg/ml; T240; Cytoskeleton) was polymerized into MTs and stabilized with Taxol following a published protocol (Westermann et al., 2005), with modifications. The incubation time was extended to 2 h. The purified Dam1C/DASH heterodecamers (1 mg/ml) were incubated with Taxol-stabilized MTs (5 mg/ml) for 20 min at 22°C. For the cryomicrotomy control, purified Dam1C/DASH heterodecamers (2.3 mg/ml) were incubated with Taxol-stabilized MTs (5 mg/ml) for 30 min at 22°C. Then, an equal volume of 80% dextran (M_r ~6,000) was added to the solution and gently mixed before self-pressurized freezing.

Plunge freezing and self-pressurized freezing of Dam1C/DASH around MTs

Dam1C/DASH-MT complexes (3 µl) were applied on the carbon side of a Quantifoil 2/2 grid (Quantifoil Micro Tools GmbH). Gold colloids (10 nm; BBI) were added as tomographic alignment

fiducials. The colloids (20 µl) were first pelleted and the supernatant was removed. Dam1C/DASH–MT complexes (3 µl) were then mixed with the gold pellet and applied to the EM grid. The grid was blotted for 2 s with force 2 and then plunged in liquid ethane using a Vitrobot (Thermo), set to 100% humidity at 4°C.

Self-pressurized freezing

Cells and cryomicrotomy control samples were self-pressurized frozen based on a previous protocol (Yakovlev and Downing, 2011). Arrested cells (50 ml) were pelleted at 5,000 g, 4°C for 5 min. The pellet was then resuspended in 1 ml of YEPD or YEPG. The cells were repelleted at 3,000 g for 1 min at 22°C, and the supernatant was discarded. Next, the cell pellet was resuspended gently in an equal volume of 50% dextran (M_r ~6,000). The resulting mixture was drawn into a copper tube (0.45-mm outer diameter) using a syringe-style loading tool (Part 733-1; Engineering Office M. Wohlwend GmbH). Both ends of the copper tubes were tightly clamped shut before being dropped into liquid ethane.

EM grid preparation for cryosections

Parallel-bar grids (G150PB-CU; EMS) with continuous carbon film were used for serial cryo-ET. The grids were plasma cleaned at 15 mA for 45 s. To coat the grids with gold fiducials, the carbon side of the grids were covered with 4 µl of a solution containing 0.1 mg/ml BSA and 10-nm gold fiducials in water (BBI). The coated grids were air-dried overnight then stored in a dry box until use.

Cryomicrotomy

All cryomicrotomy was done with a UC7 / FC7 cryomicrotome (Leica Microsystems). The frozen copper tubes were trimmed with a diamond trimming knife (Diatome) until amorphous ice was exposed. The sample was then further trimmed to produce a 130 µm × 55 µm × 30 µm (length × width × height) mesa. Next, 100-nm-thick cryosections were cut from the mesa using a 35° diamond knife (Diatome) to produce a cryoribbon, under the control of a micromanipulator (Ladinsky, 2010). The ribbon was picked up using a fiber tool and carefully placed onto an EM grid, parallel to the long bars like in Fig. 4 E, and then attached by charging with a Crion device (Leica). A laser window was sometimes used to flatten the cryoribbon on the grid. The grid was then stored in liquid nitrogen until imaged. To minimize the number of images occluded by ice contaminants, only the grids that had the minimum amount of ice contamination were used. To facilitate cryomicrotomy, we modified a published plastic cover (Studer et al., 2014) to minimize the vertical gap with the cryomicrotome chamber. We also secured an aluminum platform with a detachable metal cover (used to press cryosections onto the grid) onto the diamond knife. These two tools helped minimize the amount of ice crystal contamination.

Electron cryo-ET of in vitro Dam1C/DASH + MT

Tilt series of in vitro Dam1C/DASH + MT samples were collected using Tomo4 (Thermo). Tilt series of +60° to –60° with an increment of 2° were collected at cumulative dose of 100–130 e/Å². For defocus phase-contrast data, the nominal defocus

ranged from –10 µm to –14 µm. Tomographic reconstructions were done using the IMOD program Etomo (Kremer et al., 1996; Mastronarde, 1997; Xiong et al., 2009). All imaging parameters are reported in Table S1.

Serial electron cryo-ET

Serial cryo-ET data were collected using Tomo4. First, cryosections were imaged at low magnification (2,878×) to locate positions that showed the nucleus. Next, a single high-magnification (15,678×) projection image was recorded at a dose sufficient (1–2 e/Å²) to determine if that cell position had any spindle MTs. Successive positions centered on the same cell were located in the sequential cryosections and saved as targets for tilt series collection. Tilt series of +60° to –60° with an increment of 2° were collected at a cumulative dose of 100–130 e/Å². For defocus phase-contrast data, the nominal defocus ranged from –10 to –14 µm. For Volta phase-contrast data, the nominal defocus was –0.5 µm. See Table S1 for more details. Tomographic reconstructions and contrast transfer function compensation were done using the IMOD program Etomo (Kremer et al., 1996; Mastronarde, 1997; Xiong et al., 2009). Sequential cryotomograms were joined using Etomo.

Tomogram 3D analysis

MTs in each cryotomogram were located manually and then classified by morphology: plus ends were either blunt, tapered, or had a ram's horn configuration; the MT midsections appeared as tubes; the minus ends were conical. All MT plus ends were scrutinized for kinetochore structures. To determine the diameter of Dam1C/DASH rings, tomograms were oriented to present the en face view of Dam1C/DASH before taking the measurement. To determine distances between kMT plus ends and Dam1C/DASH rings, the tips of kMT plus ends and Dam1C/DASH rings were first treated as two discs, then the distance between the centers of both discs was taken.

To measure the Dam1C/DASH ring's radius of curvature and completeness, we first modeled each ring as a single contour in the IMOD program 3dmod. The radii of curvature were then calculated using the command: ~> imodcurvature -o 1 -rc 30,200 -m 2 -ro -st -Out [output.mod] -in [input.mod].

The circumferences were then extracted with the IMOD command: ~> imodinfo [output.mod].

As a normalization factor, we calculated the mean circumference of all complete rings, then divided in the circumferences of the individual partial rings to obtain a list of fractions of completeness. Note that we could not estimate the completeness in terms of number of decamers because the resolution of the individual rings was generally too low to count decamers.

Rotational symmetry analysis

Rotational power spectra were estimated using the python script ot_rot-ps.py (https://github.com/anaphaze/ot-tools). This script calls on EMAN2 routines to calculate correlation coefficients between the original image and copies of the image that were rotated in 1° increments (Tang et al., 2007). This correlation function is then subjected to a 1-D Fourier transform, which can then be inspected for the highest degree of symmetry.

Template matching of reconstituted Dam1C/DASH rings

PEET was used to automatically find candidate positions of all ring-shaped macromolecular complexes in cryotomograms of Dam1C/DASH reconstituted on MTs (Nicastro et al., 2006; Heumann, 2016). First, a sparse series of model points were seeded in the lumens of MTs that were encircled by Dam1C/DASH rings. Extra points were then automatically added with the curve tool of A. Noske (The University Of Queensland, St. Lucia, Australia), implemented in the IMOD program 3dmod. Two types of reference volumes were tested: (1) a lone featureless 50-nm-diameter ring and (2) this same ring encircling a short featureless 25-nm-diameter tube with 4-nm-thick walls. To minimize the effects of densities from the buffer and especially the MTs that protrude beyond the plane of the ring, the subtomograms were masked with a ~13-nm-tall, 60-nm-diameter cylinder that completely encloses the Dam1C/DASH ring. To assess the performance of the template-matching runs, the "save individual aligned particles" option was enabled in PEET. At the end of the search, overlapping hits were automatically removed by the PEET removeDuplicates routine. To minimize the number of false negatives, the correlation-cutoff was set to 0.

Subtomogram classification and averaging

Subtomogram analysis was performed using RELION 2.0 and 2.1 with the 2D and 3D classification routines (Bharat and Scheres, 2016; Kimanius et al., 2016). The centers of mass of each template-matched hits were imported in RELION. A preliminary round of 2D classification did not reveal any "junk" classes, e.g., ice crystals, contaminants, and partial rings, probably because the reference model (ring around a short tube) does not resemble the junk classes found in typical cryo-EM samples (Bharat et al., 2015). All template-matching hits were then subjected to 3D classification, using a featureless 50-nm-diameter ring as an initial reference. The influence of buffer, MT, and nearby Dam1C/DASH densities was minimized by the application of a "soft"-edged lifesaver-shaped mask (15-nm-thick, with 18- and 30-nm inner and outer radii, respectively). An initial round of asymmetric (without symmetry enforced) 3D classification revealed complete rings highly tilted to various degrees around the MT, partial rings, and spirals; the latter two classes of Dam1C/DASH assemblies were excluded from subsequent analysis. The remaining classes were very similar and had signs of 17-fold rotational symmetry. Dam1C/DASH rings belonging to the class with the clearest 17-fold symmetry were subjected to 3D autorefinement using the same mask as before and with 17-fold symmetry imposed.

For in vivo subtomogram averaging, the two most complete rings with the strongest 17-fold rotational power were aligned to a featureless 50-nm-diameter ring using PEET. 17-fold symmetry was then enforced with the Bsoft program bsym (Heymann and Belnap, 2007). A 12-nm thick ring-shaped mask was applied to eliminate the MT and nearby nucleoplasmic densities.

Figures

All cryotomographic slices were generated with the 3dmod slicer tool. Isosurface images were rendered with UCSF Chimera (Pettersen et al., 2004). Cartoons and figure layouts were composed with Adobe Illustrator and Photoshop (Adobe Systems).

Data sharing

The 17-fold-symmetrized subtomogram average of reconstituted Dam1C/DASH rings from Fig. 2 I was deposited in the EMData-Bank as EMD-6912. The serial cryotomograms that comprise the metaphase spindle from Fig. 5 B were deposited in the EMData-Bank as EMD-6914. The tilt series for all cryotomograms used to make figures in this paper were deposited in the Electron Microscopy Public Image Archive (Iudin et al., 2016) as EMPIAR-10159. This deposition includes coordinates and view angles of each in vivo Dam1C/DASH, stored in IMOD .mod files.

Online supplemental material

Fig. S1 shows cryotomographic slices of seven sequential cryosections of a metaphase yeast cell. Fig. S2 shows examples of Dam1C/DASH complexes found in cryotomograms of yeast cells used in this study, as well as the distribution Dam1C/DASH ring completeness in metaphase and Scc1-cleaved cells. Fig. S3 shows examples of Dam1C/DASH located near curved tips in vitro. Fig. S4 shows 17-fold symmetrized averages of random nuclear positions. Table S1 shows the cryo-EM imaging parameters used in this study. Video 1 shows a subtomogram average of 17-fold symmetrized Dam1C/DASH in vitro. Video 2 and Video 3 show the complete and cropped serial cryotomograms of a metaphase budding yeast cell. Video 4 shows a 3D model of a budding-yeast nucleus and spindle reconstructed by serial cryo-ET. Video 5 shows only the spindle and Dam1C/DASH from the Video 4 model, enlarged. Videos 6 and 7 show two instances of 17-fold symmetrized Dam1C/DASH rings in vivo.

References

Abad, M.A., B. Medina, A. Santamaria, J. Zou, C. Plasberg-Hill, A. Madhumalar, U. Jayachandran, P.M. Redli, J. Rappsilber, E.A. Nigg, and A.A. Jeyaprakash. 2014. Structural basis for microtubule recognition by the human kinetochore Ska complex. *Nat. Commun.* 5:2964. https://doi.org/10.1038/ncomms3964

Albert, S., M. Schaffer, F. Beck, S. Mosalaganti, S. Asano, H.F. Thomas, J.M. Plitzko, M. Beck, W. Baumeister, and B.D. Engel. 2017. Proteasomes tether to two distinct sites at the nuclear pore complex. *Proc. Natl. Acad. Sci. USA.* 114:13726–13731. https://doi.org/10.1073/pnas.1716305114

Alberts, B. 2015. Molecular biology of the cell. Garland Science, Taylor and Francis Group, New York, NY.

Alushin, G.M., V.H. Ramey, S. Pasqualato, D.A. Ball, N. Grigorieff, A. Musacchio, and E. Nogales. 2010. The Ndc80 kinetochore complex forms oligomeric arrays along microtubules. *Nature.* 467:805–810. https://doi.org/10.1038/nature09423

Aravamudhan, P., I. Felzer-Kim, K. Gurunathan, and A.P. Joglekar. 2014. Assembling the protein architecture of the budding yeast kinetochore-microtubule attachment using FRET. *Curr. Biol.* 24:1437–1446. https://doi.org/10.1016/j.cub.2014.05.014

Asbury, C.L., D.R. Gestaut, A.F. Powers, A.D. Franck, and T.N. Davis. 2006. The Dam1 kinetochore complex harnesses microtubule dynamics to produce force and movement. *Proc. Natl. Acad. Sci. USA.* 103:9873–9878. https://doi.org/10.1073/pnas.0602249103

Bäuerlein, F.J.B., I. Saha, A. Mishra, M. Kalemanov, A. Martínez-Sánchez, R. Klein, I. Dudanova, M.S. Hipp, F.U. Hartl, W. Baumeister, and R. Fernández-Busnadiego. 2017. In Situ Architecture and Cellular Interactions of PolyQ Inclusions. *Cell.* 171:179–187.e10. https://doi.org/10.1016/j.cell.2017.08.009

Bharat, T.A., and S.H. Scheres. 2016. Resolving macromolecular structures from electron cryo-tomography data using subtomogram averaging in RELION. *Nat. Protoc.* 11:2054–2065. https://doi.org/10.1038/nprot.2016.124

Bharat, T.A.M., C.J. Russo, J. Löwe, L.A. Passmore, and S.H.W. Scheres. 2015. Advances in Single-Particle Electron Cryomicroscopy Structure Determination applied to Sub-tomogram Averaging. *Structure.* 23:1743–1753. https://doi.org/10.1016/j.str.2015.06.026

Caldas, G.V., and J.G. DeLuca. 2014. KNL1: bringing order to the kinetochore. *Chromosoma.* 123:169–181. https://doi.org/10.1007/s00412-013-0446-5

Chang, Y.W., S. Chen, E.I. Tocheva, A. Treuner-Lange, S. Löbach, L. Søgaard-Andersen, and G.J. Jensen. 2014. Correlated cryogenic photoactivated localization microscopy and cryo-electron tomography. *Nat. Methods.* 11:737–739. https://doi.org/10.1038/nmeth.2961

Cheeseman, I.M., M. Enquist-Newman, T. Müller-Reichert, D.G. Drubin, and G. Barnes. 2001. Mitotic spindle integrity and kinetochore function linked by the Duo1p/Dam1p complex. *J. Cell Biol.* 152:197–212. https://doi.org/10.1083/jcb.152.1.197

Chen, C., H.H. Lim, J. Shi, S. Tamura, K. Maeshima, U. Surana, and L. Gan. 2016. Budding yeast chromatin is dispersed in a crowded nucleoplasm in vivo. *Mol. Biol. Cell.* 27:3357–3368. https://doi.org/10.1091/mbc.e16-07-0506

Dhatchinamoorthy, K., M. Shivaraju, J.J. Lange, B. Rubinstein, J.R. Unruh, B.D. Slaughter, and J.L. Gerton. 2017. Structural plasticity of the living kinetochore. *J. Cell Biol.* 216:3551–3570. https://doi.org/10.1083/jcb.201703152

Dimitrova, Y.N., S. Jenni, R. Valverde, Y. Khin, and S.C. Harrison. 2016. Structure of the MIND Complex Defines a Regulatory Focus for Yeast Kinetochore Assembly. *Cell.* 167:1014–1027.e12. https://doi.org/10.1016/j.cell.2016.10.011

Efremov, A., E.L. Grishchuk, J.R. McIntosh, and F.I. Ataullakhanov. 2007. In search of an optimal ring to couple microtubule depolymerization to processive chromosome motions. *Proc. Natl. Acad. Sci. USA.* 104:19017–19022. https://doi.org/10.1073/pnas.0709524104

Franck, A.D., A.F. Powers, D.R. Gestaut, T. Gonen, T.N. Davis, and C.L. Asbury. 2007. Tension applied through the Dam1 complex promotes microtubule elongation providing a direct mechanism for length control in mitosis. *Nat. Cell Biol.* 9:832–837. https://doi.org/10.1038/ncb1609

Gan, L., M.S. Ladinsky, and G.J. Jensen. 2011. Organization of the smallest eukaryotic spindle. *Curr. Biol.* 21:1578–1583. https://doi.org/10.1016/j.cub.2011.08.021

Gestaut, D.R., B. Graczyk, J. Cooper, P.O. Widlund, A. Zelter, L. Wordeman, C.L. Asbury, and T.N. Davis. 2008. Phosphoregulation and depolymerization-driven movement of the Dam1 complex do not require ring formation. *Nat. Cell Biol.* 10:407–414. https://doi.org/10.1038/ncb1702

Gillett, E.S., C.W. Espelin, and P.K. Sorger. 2004. Spindle checkpoint proteins and chromosome-microtubule attachment in budding yeast. *J. Cell Biol.* 164:535–546. https://doi.org/10.1083/jcb.200308100

Gonen, S., B. Akiyoshi, M.G. Iadanza, D. Shi, N. Duggan, S. Biggins, and T. Gonen. 2012. The structure of purified kinetochores reveals multiple microtubule-attachment sites. *Nat. Struct. Mol. Biol.* 19:925–929. https://doi.org/10.1038/nsmb.2358

Goshima, G., and M. Yanagida. 2000. Establishing biorientation occurs with precocious separation of the sister kinetochores, but not the arms, in the early spindle of budding yeast. *Cell.* 100:619–633. https://doi.org/10.1016/S0092-8674(00)80699-6

Grishchuk, E.L., I.S. Spiridonov, V.A. Volkov, A. Efremov, S. Westermann, D. Drubin, G. Barnes, F.I. Ataullakhanov, and J.R. McIntosh. 2008. Different assemblies of the DAM1 complex follow shortening microtubules by distinct mechanisms. *Proc. Natl. Acad. Sci. USA.* 105:6918–6923. https://doi.org/10.1073/pnas.0801811105

Hanisch, A., H.H.W. Silljé, and E.A. Nigg. 2006. Timely anaphase onset requires a novel spindle and kinetochore complex comprising Ska1 and Ska2. *EMBO J.* 25:5504–5515. https://doi.org/10.1038/sj.emboj.7601426

Heumann, J.M. 2016. PEET. University of Colorado Boulder. Available at: http://bio3d.colorado.edu/PEET/ (accessed January 1, 2018).

Heymann, J.B., and D.M. Belnap. 2007. Bsoft: image processing and molecular modeling for electron microscopy. *J. Struct. Biol.* 157:3–18. https://doi.org/10.1016/j.jsb.2006.06.006

Higuchi, T., and F. Uhlmann. 2005. Stabilization of microtubule dynamics at anaphase onset promotes chromosome segregation. *Nature.* 433:171–176. https://doi.org/10.1038/nature03240

Hill, T.L. 1985. Theoretical problems related to the attachment of microtubules to kinetochores. *Proc. Natl. Acad. Sci. USA.* 82:4404–4408. https://doi.org/10.1073/pnas.82.13.4404

Hofmann, C., I.M. Cheeseman, B.L. Goode, K.L. McDonald, G. Barnes, and D.G. Drubin. 1998. Saccharomyces cerevisiae Duo1p and Dam1p, novel proteins involved in mitotic spindle function. *J. Cell Biol.* 143:1029–1040. https://doi.org/10.1083/jcb.143.4.1029

Iudin, A., P.K. Korir, J. Salavert-Torres, G.J. Kleywegt, and A. Patwardhan. 2016. EMPIAR: a public archive for raw electron microscopy image data. *Nat. Methods.* 13:387–388. https://doi.org/10.1038/nmeth.3806

Janczyk, P.Ł., K.A. Skorupka, J.G. Tooley, D.R. Matson, C.A. Kestner, T. West, O. Pornillos, and P.T. Stukenberg. 2017. Mechanism of Ska Recruitment by Ndc80 Complexes to Kinetochores. *Dev. Cell.* 41:438–449.e4. https://doi.org/10.1016/j.devcel.2017.04.020

Janke, C., J. Ortíz, T.U. Tanaka, J. Lechner, and E. Schiebel. 2002. Four new subunits of the Dam1-Duo1 complex reveal novel functions in sister kinetochore biorientation. *EMBO J.* 21:181–193. https://doi.org/10.1093/emboj/21.1.181

Jenni, S., and S.C. Harrison. 2018. Structure of the DASH/Dam1 complex shows its role at the yeast kinetochore-microtubule interface. *Science.* 360:552–558. https://doi.org/10.1126/science.aar6436

Jin, Q.W., J. Fuchs, and J. Loidl. 2000. Centromere clustering is a major determinant of yeast interphase nuclear organization. *J. Cell Sci.* 113:1903–1912.

Joglekar, A.P., and A.A. Kukreja. 2017. How Kinetochore Architecture Shapes the Mechanisms of Its Function. *Curr. Biol.* 27:R816–R824. https://doi.org/10.1016/j.cub.2017.06.012

Joglekar, A.P., D.C. Bouck, J.N. Molk, K.S. Bloom, and E.D. Salmon. 2006. Molecular architecture of a kinetochore-microtubule attachment site. *Nat. Cell Biol.* 8:581–585. https://doi.org/10.1038/ncb1414

Joglekar, A.P., D. Bouck, K. Finley, X. Liu, Y. Wan, J. Berman, X. He, E.D. Salmon, and K.S. Bloom. 2008. Molecular architecture of the kinetochore-microtubule attachment site is conserved between point and regional centromeres. *J. Cell Biol.* 181:587–594. https://doi.org/10.1083/jcb.200803027

Joglekar, A.P., K. Bloom, and E.D. Salmon. 2009. In vivo protein architecture of the eukaryotic kinetochore with nanometer scale accuracy. *Curr. Biol.* 19:694–699. https://doi.org/10.1016/j.cub.2009.02.056

Jones, M.H., J.B. Bachant, A.R. Castillo, T.H. Giddings Jr., and M. Winey. 1999. Yeast Dam1p is required to maintain spindle integrity during mito-

sis and interacts with the Mps1p kinase. *Mol. Biol. Cell.* 10:2377–2391. https://doi.org/10.1091/mbc.10.7.2377

Kimanius, D., B.O. Forsberg, S.H. Scheres, and E. Lindahl. 2016. Accelerated cryo-EM structure determination with parallelisation using GPUs in RELION-2. *eLife.* 5:e18722. https://doi.org/10.7554/eLife.18722

Kitamura, E., K. Tanaka, Y. Kitamura, and T.U. Tanaka. 2007. Kinetochore microtubule interaction during S phase in Saccharomyces cerevisiae. *Genes Dev.* 21:3319–3330. https://doi.org/10.1101/gad.449407

Kremer, J.R., D.N. Mastronarde, and J.R. McIntosh. 1996. Computer visualization of three-dimensional image data using IMOD. *J. Struct. Biol.* 116:71–76. https://doi.org/10.1006/jsbi.1996.0013

Krishnan, V., S. Nirantar, K. Crasta, A.Y. Cheng, and U. Surana. 2004. DNA replication checkpoint prevents precocious chromosome segregation by regulating spindle behavior. *Mol. Cell.* 16:687–700. https://doi.org/10.1016/j.molcel.2004.11.001

Ladinsky, M.S. 2010. Micromanipulator-assisted vitreous cryosectioning and sample preparation by high-pressure freezing. *Methods Enzymol.* 481:165–194. https://doi.org/10.1016/S0076-6879(10)81008-0

Lau, D.T., and A.W. Murray. 2012. Mad2 and Mad3 cooperate to arrest budding yeast in mitosis. *Curr. Biol.* 22:180–190. https://doi.org/10.1016/j.cub.2011.12.029

Legal, T., J. Zou, A. Sochaj, J. Rappsilber, and J.P.I. Welburn. 2016. Molecular architecture of the Dam1 complex-microtubule interaction. *Open Biol.* 6:150237. https://doi.org/10.1098/rsob.150237

Li, Y., J. Bachant, A.A. Alcasabas, Y. Wang, J. Qin, and S.J. Elledge. 2002. The mitotic spindle is required for loading of the DASH complex onto the kinetochore. *Genes Dev.* 16:183–197. https://doi.org/10.1101/gad.959402

Liang, H., H.H. Lim, A. Venkitaraman, and U. Surana. 2012. Cdk1 promotes kinetochore bi-orientation and regulates Cdc20 expression during recovery from spindle checkpoint arrest. *EMBO J.* 31:403–416. https://doi.org/10.1038/emboj.2011.385

Mastronarde, D.N. 1997. Dual-axis tomography: an approach with alignment methods that preserve resolution. *J. Struct. Biol.* 120:343–352. https://doi.org/10.1006/jsbi.1997.3919

McEwen, B.F., C.E. Hsieh, A.L. Mattheyses, and C.L. Rieder. 1998. A new look at kinetochore structure in vertebrate somatic cells using high-pressure freezing and freeze substitution. *Chromosoma.* 107:366–375. https://doi.org/10.1007/s004120050320

McIntosh, J.R. 2005. Rings around kinetochore microtubules in yeast. *Nat. Struct. Mol. Biol.* 12:210–212. https://doi.org/10.1038/nsmb0305-210

McIntosh, J.R., E. O'Toole, K. Zhudenkov, M. Morphew, C. Schwartz, F.I. Ataullakhanov, and E.L. Grishchuk. 2013. Conserved and divergent features of kinetochores and spindle microtubule ends from five species. *J. Cell Biol.* 200:459–474. https://doi.org/10.1083/jcb.201209154

McIntosh, J.R., E. O'Toole, G. Morgan, J. Austin, E. Ulyanov, F. Ataullakhanov, and N. Gudimchuk. 2018. Microtubules grow by the addition of bent guanosine triphosphate tubulin to the tips of curved protofilaments. *J. Cell Biol.* 217:2691–2708. https://doi.org/10.1083/jcb.201802138

Michaelis, C., R. Ciosk, and K. Nasmyth. 1997. Cohesins: chromosomal proteins that prevent premature separation of sister chromatids. *Cell.* 91:35–45. https://doi.org/10.1016/S0092-8674(01)80007-6

Miranda, J.J., P. De Wulf, P.K. Sorger, and S.C. Harrison. 2005. The yeast DASH complex forms closed rings on microtubules. *Nat. Struct. Mol. Biol.* 12:138–143. https://doi.org/10.1038/nsmb896

Miranda, J.J., D.S. King, and S.C. Harrison. 2007. Protein arms in the kinetochore-microtubule interface of the yeast DASH complex. *Mol. Biol. Cell.* 18:2503–2510. https://doi.org/10.1091/mbc.e07-02-0135

Mirchenko, L., and F. Uhlmann. 2010. Sli15(INCENP) dephosphorylation prevents mitotic checkpoint reengagement due to loss of tension at anaphase onset. *Curr. Biol.* 20:1396–1401. https://doi.org/10.1016/j.cub.2010.06.023

Murphy, G.E., J.R. Leadbetter, and G.J. Jensen. 2006. In situ structure of the complete Treponema primitia flagellar motor. *Nature.* 442:1062–1064. https://doi.org/10.1038/nature05015

Musacchio, A., and A. Desai. 2017. A Molecular View of Kinetochore Assembly and Function. *Biology (Basel).* 6:5.

Musacchio, A., and E.D. Salmon. 2007. The spindle-assembly checkpoint in space and time. *Nat. Rev. Mol. Cell Biol.* 8:379–393. https://doi.org/10.1038/nrm2163

Nicastro, D., C. Schwartz, J. Pierson, R. Gaudette, M.E. Porter, and J.R. McIntosh. 2006. The molecular architecture of axonemes revealed by cryo-electron tomography. *Science.* 313:944–948. https://doi.org/10.1126/science.1128618

Nogales, E., and V.H. Ramey. 2009. Structure-function insights into the yeast Dam1 kinetochore complex. *J. Cell Sci.* 122:3831–3836. https://doi.org/10.1242/jcs.004689

O'Toole, E.T., D.N. Mastronarde, T.H. Giddings Jr., M. Winey, D.J. Burke, and J.R. McIntosh. 1997. Three-dimensional analysis and ultrastructural design of mitotic spindles from the cdc20 mutant of Saccharomyces cerevisiae. *Mol. Biol. Cell.* 8:1–11. https://doi.org/10.1091/mbc.8.1.1

Pettersen, E.F., T.D. Goddard, C.C. Huang, G.S. Couch, D.M. Greenblatt, E.C. Meng, and T.E. Ferrin. 2004. UCSF Chimera--a visualization system for exploratory research and analysis. *J. Comput. Chem.* 25:1605–1612. https://doi.org/10.1002/jcc.20084

Ramey, V.H., H.-W. Wang, Y. Nakajima, A. Wong, J. Liu, D. Drubin, G. Barnes, and E. Nogales. 2011. The Dam1 ring binds to the E-hook of tubulin and diffuses along the microtubule. *Mol. Biol. Cell.* 22:457–466. https://doi.org/10.1091/mbc.e10-10-0841

Richmond, D., R. Rizkallah, F. Liang, M.M. Hurt, and Y. Wang. 2013. Slk19 clusters kinetochores and facilitates chromosome bipolar attachment. *Mol. Biol. Cell.* 24:566–577. https://doi.org/10.1091/mbc.e12-07-0552

Studer, D., A. Klein, I. Iacovache, H. Gnaegi, and B. Zuber. 2014. A new tool based on two micromanipulators facilitates the handling of ultrathin cryosection ribbons. *J. Struct. Biol.* 185:125–128. https://doi.org/10.1016/j.jsb.2013.11.005

Tachiwana, H., W. Kagawa, T. Shiga, A. Osakabe, Y. Miya, K. Saito, Y. Hayashi-Takanaka, T. Oda, M. Sato, S.Y. Park, et al. 2011. Crystal structure of the human centromeric nucleosome containing CENP-A. *Nature.* 476:232–235. https://doi.org/10.1038/nature10258

Tanaka, T.U. 2010. Kinetochore-microtubule interactions: steps towards bi-orientation. *EMBO J.* 29:4070–4082. https://doi.org/10.1038/emboj.2010.294

Tanaka, K., N. Mukae, H. Dewar, M. van Breugel, E.K. James, A.R. Prescott, C. Antony, and T.U. Tanaka. 2005. Molecular mechanisms of kinetochore capture by spindle microtubules. *Nature.* 434:987–994. https://doi.org/10.1038/nature03483

Tanaka, K., E. Kitamura, Y. Kitamura, and T.U. Tanaka. 2007. Molecular mechanisms of microtubule-dependent kinetochore transport toward spindle poles. *J. Cell Biol.* 178:269–281. https://doi.org/10.1083/jcb.200702141

Tang, G., L. Peng, P.R. Baldwin, D.S. Mann, W. Jiang, I. Rees, and S.J. Ludtke. 2007. EMAN2: an extensible image processing suite for electron microscopy. *J. Struct. Biol.* 157:38–46. https://doi.org/10.1016/j.jsb.2006.05.009

Uhlmann, F., D. Wernic, M.A. Poupart, E.V. Koonin, and K. Nasmyth. 2000. Cleavage of cohesin by the CD clan protease separin triggers anaphase in yeast. *Cell.* 103:375–386. https://doi.org/10.1016/S0092-8674(00)00130-6

van Hooff, J.J.E., B. Snel, and G.J.P.L. Kops. 2017. Unique Phylogenetic Distributions of the Ska and Dam1 Complexes Support Functional Analogy and Suggest Multiple Parallel Displacements of Ska by Dam1. *Genome Biol. Evol.* 9:1295–1303. https://doi.org/10.1093/gbe/evx088

Volkov, V.A., A.V. Zaytsev, N. Gudimchuk, P.M. Grissom, A.L. Gintsburg, F.I. Ataullakhanov, J.R. McIntosh, and E.L. Grishchuk. 2013. Long tethers provide high-force coupling of the Dam1 ring to shortening microtubules. *Proc. Natl. Acad. Sci. USA.* 110:7708–7713. https://doi.org/10.1073/pnas.1305821110

Wang, H.-W., V.H. Ramey, S. Westermann, A.E. Leschziner, J.P.I. Welburn, Y. Nakajima, D.G. Drubin, G. Barnes, and E. Nogales. 2007. Architecture of the Dam1 kinetochore ring complex and implications for microtubule-driven assembly and force-coupling mechanisms. *Nat. Struct. Mol. Biol.* 14:721–726. https://doi.org/10.1038/nsmb1274

Wang, H.W., S. Long, C. Ciferri, S. Westermann, D. Drubin, G. Barnes, and E. Nogales. 2008. Architecture and flexibility of the yeast Ndc80 kinetochore complex. *J. Mol. Biol.* 383:894–903. https://doi.org/10.1016/j.jmb.2008.08.077

Welburn, J.P.I., E.L. Grishchuk, C.B. Backer, E.M. Wilson-Kubalek, J.R. Yates III, and I.M. Cheeseman. 2009. The human kinetochore Ska1 complex facilitates microtubule depolymerization-coupled motility. *Dev. Cell.* 16:374–385. https://doi.org/10.1016/j.devcel.2009.01.011

Westermann, S., A. Avila-Sakar, H.-W. Wang, H. Niederstrasser, J. Wong, D.G. Drubin, E. Nogales, and G. Barnes. 2005. Formation of a dynamic kinetochore- microtubule interface through assembly of the Dam1 ring complex. *Mol. Cell.* 17:277–290. https://doi.org/10.1016/j.molcel.2004.12.019

Westermann, S., H.-W. Wang, A. Avila-Sakar, D.G. Drubin, E. Nogales, and G. Barnes. 2006. The Dam1 kinetochore ring complex moves processively on depolymerizing microtubule ends. *Nature.* 440:565–569. https://doi.org/10.1038/nature04409

Winey, M., C.L. Mamay, E.T. O'Toole, D.N. Mastronarde, T.H. Giddings Jr., K.L. McDonald, and J.R. McIntosh. 1995. Three-dimensional ultrastructural analysis of the Saccharomyces cerevisiae mitotic spindle. *J. Cell Biol.* 129:1601–1615. https://doi.org/10.1083/jcb.129.6.1601

Xiong, Q., M.K. Morphew, C.L. Schwartz, A.H. Hoenger, and D.N. Mastronarde. 2009. CTF determination and correction for low dose tomographic tilt series. *J. Struct. Biol.* 168:378–387. https://doi.org/10.1016/j.jsb.2009.08.016

Yakovlev, S., and K.H. Downing. 2011. Freezing in sealed capillaries for preparation of frozen hydratedsections. *J. Microsc.* 244:235–247. https://doi.org/10.1111/j.1365-2818.2011.03530.x

Zelter, A., M. Bonomi, J. Kim, N.T. Umbreit, M.R. Hoopmann, R. Johnson, M. Riffle, D. Jaschob, M.J. MacCoss, R.L. Moritz, and T.N. Davis. 2015. The molecular architecture of the Dam1 kinetochore complex is defined by cross-linking based structural modelling. *Nat. Commun.* 6:8673. https://doi.org/10.1038/ncomms9673

Zhang, Q., S. Sivakumar, Y. Chen, H. Gao, L. Yang, Z. Yuan, H. Yu, and H. Liu. 2017. Ska3 Phosphorylated by Cdk1 Binds Ndc80 and Recruits Ska to Kinetochores to Promote Mitotic Progression. *Curr. Biol.* 27:1477–1484.e4. https://doi.org/10.1016/j.cub.2017.03.060